Manuscript prepared for Atmos. Chem. Phys.
with version 2015/04/24 7.83 Copernicus papers of the LATEX class copernicus.cls.
Date: 29 June 2016

A multi-model intercomparison of halogenated very short-lived substances (TransCom-VSLS): linking oceanic emissions and tropospheric transport for a reconciled estimate of the stratospheric source gas injection of bromine

R. Hossaini[1,a], P. K. Patra[2], A. A Leeson[1,b], G. Krysztofiak[3,c], N. L. Abraham[4,5], S. J. Andrews[6], A. T. Archibald[4], J. Aschmann[7], E. L. Atlas[8], D. A. Belikov[9,10,11], H. Bönisch[12], L. J. Carpenter[6], S. Dhomse[1], M. Dorf[13], A. Engel[12], W. Feng[1,4], S. Fuhlbrügge[14], P. T. Griffiths[5], N. R. P. Harris[5], R. Hommel[7], T. Keber[12], K. Krüger[14,15], S. T. Lennartz[14], S. Maksyutov[9], H. Mantle[1], G. P. Mills[16], B. Miller[17], S. A. Montzka[17], F. Moore[17], M. A. Navarro[8], D. E. Oram[16], K. Pfeilsticker[18], J. A. Pyle[4,5], B. Quack[14], A. D. Robinson[5], E. Saikawa[19,20], A. Saiz-Lopez[21], S. Sala[12], B.-M Sinnhuber[3], S. Taguchi[22], S. Tegtmeier[14], R. T. Lidster[6], C. Wilson[1,23], and F. Ziska[14]

[1]School of Earth and Environment, University of Leeds, Leeds, UK.
[2]Department of Environmental Geochemical Cycle Research, JAMSTEC, Yokohama, Japan.
[3]Institute for Meteorology and Climate Research, Karlsruhe Institute of Technology, Karlsruhe, Germany.
[4]National Centre for Atmospheric Science, UK.
[5]Department of Chemistry, University of Cambridge, Cambridge, UK.
[6]Department of Chemistry, University of York, Heslington, York, UK.
[7]Institute of Environmental Physics, University of Bremen, Bremen, Germany.
[8]Rosenstiel School of Marine and Atmospheric Science, University of Miami, USA.
[9]Center for Global Environmental Research, National Institute for Environmental Studies, Tsukuba, Japan.
[10]National Institute of Polar Research, Tokyo, Japan.
[11]Tomsk State University, Tomsk, Russia.
[12]Institute for Atmospheric and Environmental Sciences, Universität Frankfurt/Main, Germany.
[13]Max-Planck-Institute for Chemistry, Mainz, Germany.
[14]GEOMAR Helmholtz Centre for Ocean Research Kiel, Kiel, Germany.
[15]University of Oslo, Department of Geosciences, Oslo, Norway.
[16]School of Environmental Sciences, University of East Anglia, Norwich, UK.
[17]National Oceanic and Atmospheric Administration, Boulder, USA.
[18]Institute for Environmental Physics, University of Heidelberg, Heidelberg, Germany.
[19]Department of Environmental Sciences, Emory University, Atlanta, USA.
[20]Department of Environmental Health, Rollins School of Public Health, Emory University, Atlanta, USA.
[21]Atmospheric Chemistry and Climate Group, Institute of Physical Chemistry Rocasolano, CSIC, Madrid, Spain.
[22]National Institute of Advanced Industrial Science and Technology, Japan.
[23]National Centre for Earth Observation, Leeds, UK.
[a]now at: Lancaster Environment Centre, Lancaster University, Lancaster, UK.

[b]now at: Lancaster Environment Centre / Data Science Institute, Lancaster University, Lancaster, UK.

[c]now at: Laboratoire de Physique et Chimie de l'Environnement et de l'Espace, CNRS-Université d'Orléans, Orléans, France.

Correspondence to: Ryan Hossaini
(r.hossaini@leeds.ac.uk)

Abstract. The first concerted multi-model intercomparison of halogenated very short-lived substances (VSLS) has been performed, within the framework of the ongoing Atmospheric Tracer Transport Model Intercomparison Project (TransCom). Eleven global models or model variants participated (nine chemical transport models and two chemistry-climate models) by simulating the major natural bromine VSLS, bromoform ($CHBr_3$) and dibromomethane (CH_2Br_2), over a 20-year period (1993-2012). Except for 3 model simulations, all others were driven offline by (or nudged to) reanalysed meteorology. The overarching goal of TransCom-VSLS was to provide a reconciled model estimate of the stratospheric source gas injection (SGI) of bromine from these gases, to constrain the current measurement-derived range, and to investigate inter-model differences due to emissions and transport processes. Models ran with standardised idealised chemistry, to isolate differences due to transport, and we investigated the sensitivity of results to a range of VSLS emission inventories. Models were tested in their ability to reproduce the observed seasonal and spatial distribution of VSLS at the surface, using measurements from NOAA's long-term global monitoring network, and in the tropical troposphere, using recent aircraft measurements - including high altitude observations from the NASA Global Hawk platform.

The models generally capture the observed seasonal cycle of surface $CHBr_3$ and CH_2Br_2 well, with a strong model-measurement correlation ($r \geq 0.7$) at most sites. In a given model, the absolute model-measurement agreement at the surface is highly sensitive to the choice of emissions. Large inter-model differences are apparent when using the same emission inventory, highlighting the challenges faced in evaluating such inventories at the global scale. Across the ensemble, most consistency is found within the tropics where most of the models (8 out of 11) achieve best agreement to surface $CHBr_3$ observations using the lowest of the three $CHBr_3$ emission inventories tested (similarly, 8 out of 11 models for CH_2Br_2). In general, the models reproduce well observations of $CHBr_3$ and CH_2Br_2 obtained in the tropical tropopause layer (TTL) at various locations throughout the Pacific. Zonal variability in VSLS loading in the TTL is generally consistent among models, with $CHBr_3$ (and to a lesser extent CH_2Br_2) most elevated over the tropical West Pacific during boreal winter. The models also indicate the Asian Monsoon during boreal summer to be an important pathway for VSLS reaching the stratosphere, though the strength of this signal varies considerably among models.

We derive an ensemble climatological mean estimate of the stratospheric bromine SGI from $CHBr_3$ and CH_2Br_2 of 2.0 (1.2-2.5) ppt, ∼57% larger than the best estimate from the most recent World Meteorological Organization (WMO) Ozone Assessment Report. We find no evidence for a long-term, transport-driven trend in the stratospheric SGI of bromine over the simulation period. The transport-driven inter-annual variability in the annual mean bromine SGI is of the order of ±5%, with SGI exhibiting a strong positive correlation with ENSO in the East Pacific. Overall, our results do not show systematic differences between models specific to the choice of reanalysis me-

teorology, rather clear differences are seen related to differences in the implementation of transport processes in the models.

1 Introduction

40 Halogenated very short-lived substances (VSLS) are gases with atmospheric lifetimes shorter than, or comparable to, tropospheric transport timescales ($\sim$6 months or less at the surface). Naturally-emitted VSLS, such as bromoform ($CHBr_3$), have marine sources and are produced by phytoplankton (e.g. Quack and Wallace, 2003) and various species of seaweed (e.g. Carpenter and Liss, 2000) - a number of which are farmed for commercial application (Leedham et al., 2013). Once in the at-

45 mosphere, VSLS (and their degradation products) may ascend to the lower stratosphere (LS), where they contribute to the inorganic bromine (Br_y) budget (e.g. Pfeilsticker et al., 2000; Sturges et al., 2000) and thereby enhance halogen-driven ozone (O_3) loss (Salawitch et al., 2005; Feng et al., 2007; Sinnhuber et al., 2009; Sinnhuber and Meul, 2015). On a per molecule basis, O_3 perturbations near the tropopause exert the largest radiative effect (e.g. Lacis et al., 1990; Forster and Shine, 1997;

50 Riese et al., 2012) and recent work has highlighted the climate relevance of VSLS-driven O_3 loss in this region (Hossaini et al., 2015a).

Quantifying the contribution of VSLS to stratospheric Br_y (Br_y^{VSLS}) has been a major objective of numerous recent observational studies (e.g. Dorf et al., 2008; Laube et al., 2008; Brinckmann et al., 2012; Sala et al., 2014; Wisher et al., 2014) and modelling efforts (e.g. Warwick et al., 2006; Hossaini et al.,

55 2010; Liang et al., 2010; Aschmann et al., 2011; Tegtmeier et al., 2012; Hossaini et al., 2012b, 2013; Aschmann and Sinnhuber, 2013; Fernandez et al., 2014). However, despite a wealth of research, Br_y^{VSLS} remains poorly constrained, with a current best-estimate range of 2-8 ppt reported in the most recent World Meteorological Organization (WMO) Ozone Assessment Report (Carpenter and Reimann, 2014). Between 15% and 76% of this supply comes from the stratospheric *source gas injection*

60 (SGI) of VSLS; i.e. the transport of a source gas (e.g. $CHBr_3$) across the tropopause, followed by its breakdown and in-situ release of Br_y^{VSLS} in the LS. The remainder comes from the troposphere-to-stratosphere transport of both organic and inorganic product gases, formed following the breakdown of VSLS below the tropopause; termed *product gas injection* (PGI).

Owing to their short tropospheric lifetimes, combined with significant spatial and temporal inho-

65 mogeneity in their emissions (e.g. Carpenter et al., 2005; Archer et al., 2007; Orlikowska and Schulz-Bull, 2009; Ziska et al., 2013; Stemmler et al., 2015), the atmospheric abundance of VSLS can exhibit sharp tropospheric gradients. The stratospheric SGI of VSLS is expected to be most efficient in regions where strong uplift, such as convectively active regions, coincides with regions of elevated surface mixing ratios (e.g. Tegtmeier et al., 2012, 2013; Liang et al., 2014), driven by strong lo-

70 calised emissions or "hot spots". Both the magnitude and distribution of emissions, with respect to transport processes, could be, therefore, an important determining factor for SGI. However, current

global-scale emission inventories of $CHBr_3$ and CH_2Br_2 are poorly constrained, owing to a paucity of observations used to derive their surface fluxes (Ashfold et al., 2014), contributing significant uncertainty to model estimates of Br_y^{VSLS} (Hossaini et al., 2013). Given the uncertainties outlined above, it is unclear how well preferential transport pathways of VSLS to the LS are represented in global scale models.

Strong convective source regions, such as the tropical West Pacific during boreal winter, are likely important for the troposphere-to-stratosphere transport of VSLS (e.g. Levine et al., 2007; Aschmann et al., 2009; Pisso et al., 2010; Hossaini et al., 2012b; Liang et al., 2014). The Asian Monsoon also represents an effective pathway for boundary layer air to be rapidly transported to the LS (e.g. Randel et al., 2010; Vogel et al., 2014; Orbe et al., 2015; Tissier and Legras , 2016), though its importance for the troposphere-to-stratosphere transport of VSLS is largely unknown, owing to a lack of observations in the region. While global models simulate broadly similar features in the spatial distribution of convection, large inter-model differences in the amount of tracers transported to the tropopause have been reported by Hoyle et al. (2011), who performed a model intercomparison of idealised ("VSLS-like") tracers with a uniform surface distribution. In order for a robust estimate of the stratospheric SGI of bromine, it is necessary to consider spatial variations in VSLS emissions, and how such variations couple with transport processes. However, a concerted model evaluation of this type has yet to be performed.

Over a series of two papers, we present results from the first VSLS multi-model intercomparison project (TransCom-VSLS). The TransCom initiative was setup in the 1990s to examine the performance of chemical transport models. Previous TransCom studies have examined non-reactive tropospheric species, such as sulphur hexafluoride (SF_6) (Denning et al., 1999) and carbon dioxide (CO_2) (Law et al., 1996, 2008). Most recently, TransCom projects have examined the influence of emissions, transport and chemical loss on atmospheric CH_4 (Patra et al., 2011) and N_2O (Thompson et al., 2014). The overarching goal of TransCom-VSLS was to constrain estimates of Br_y^{VSLS}, towards closure of the stratospheric bromine budget, by (i) providing a reconciled climatological model estimate of bromine SGI, to reduce uncertainty on the measurement-derived range (0.7-3.4 ppt Br) - currently uncertain by a factor of $\sim$5 (Carpenter and Reimann, 2014) - and (ii) quantify the influence of emissions and transport processes on inter-model differences in SGI. In this regard, we define *transport* differences between models as the effects of boundary layer mixing, convection and advection, and the implementation of these processes. The project was not designed to separate clearly the contributions of each transport component in the large model ensemble, but can be inferred as the boundary layer mixing affects tracer concentrations mainly near the surface, convection controls tracer transport to the upper troposphere and advection mainly distributes tracers horizontally (e.g. Patra et al., 2009). Specific objectives were to (a) evaluate models against measurements from the surface to the tropical tropopause layer (TTL) and (b) examine zonal and seasonal variations in VSLS loading in the TTL. We also show inter-annual variability in the strato-

spheric loading of VSLS (limited to transport) and briefly discuss possible trends related to the El

110 Niño Southern Oscillation (ENSO). Section 2 gives a description of the experimental design and an overview of participating models. Model-measurement comparisons are given in Sections 3.1 to 3.3. Section 3.4 examines zonal/seasonal variations in the troposphere-stratosphere transport of VSLS and Section 3.5 provides our reconciled estimate of bromine SGI and discusses inter-annual variability.

2   Methods, Models and Observations

Eleven models, or their variants, took part in TransCom-VSLS. Each model simulated the major bromine VSLS, bromoform ($CH Br_3$) and dibromomethane ($CH_2 Br_2$), which together account for 77-86% of the total bromine SGI from VSLS reaching the stratosphere (Carpenter and Reimann, 2014). Participating models also simulated the major iodine VSLS, methyl iodide ($CH_3 I$), though

120 results from the iodine simulations will feature in a forthcoming, stand-alone paper (Hossaini et al. 2016, in prep). Each model ran with multiple $CH Br_3$ and $CH_2 Br_2$ emission inventories (see Section 2.1) in order to (i) investigate the performance of each inventory, in a given model, against observations and (ii) identify potential inter-model differences whilst using the same inventory. Analogous to previous TransCom experiments (e.g. Patra et al., 2011), a standardised treatment of tropospheric

125 chemistry was employed, through use of prescribed oxidants and photolysis rates (see Section 2.2). This approach (i) ensured a consistent chemical sink of VSLS among models, minimising the influence of inter-model differences in tropospheric chemistry on the results, and thereby (ii) isolated differences due to transport processes. Long-term simulations, over a 20 year period (1993-2012), were performed by each model in order to examine trends and transport-driven inter-annual vari-

130 ability in the stratospheric SGI of $CH Br_3$ and $CH_2 Br_2$. Global monthly mean model output over the full simulation period, along with output at a higher temporal resolution (typically hourly) over measurement campaign periods, was requested from each group. A brief description of the models is given in Section 2.3 and a description of the observational data used in this work is given in Section 2.4. Figure 1 summarises the approach of TransCom-VSLS and its broad objectives.

2.1   Tracers and oceanic emission fluxes

Owing to significant differences in the magnitude and spatial distribution of VSLS emission fluxes, among previously published inventories (Hossaini et al., 2013), all models ran with multiple $CH Br_3$ and $CH_2 Br_2$ tracers. Each of these tracers used a different set of prescribed surface emissions. Tracers named "$CH Br_3\_L$", "$CH Br_3\_O$" and "$CH Br_3\_Z$" used the inventories of Liang et al. (2010),

140 Ordóñez et al. (2012) and Ziska et al. (2013), respectively. These three studies also reported emission fluxes for $CH_2 Br_2$, and thus the same (L/O/Z) notation applies to the model $CH_2 Br_2$ tracers, as summarised in Table 1. As these inventories were recently described and compared by Hossaini et al.

(2013), only a brief description of each is given below. Surface $CHBr_3$/CH_2Br_2 emission maps for each inventory are given in the Supplementary Information (Figures S1 and S2).

145   The Liang et al. (2010) inventory is a top-down estimate of VSLS emissions based on aircraft observations, mostly concentrated around the Pacific and North America between 1996 and 2008. Measurements of $CHBr_3$ and CH_2Br_2 from the following National Aeronautics and Space Administration (NASA) aircraft campaigns were used to derive the ocean fluxes: PEM-Tropics, TRACE-P, INTEX, TC4, ARCTAS, STRAT, Pre-AVE and AVE. This inventory is aseasonal and assumes the

150   same spatial distribution of emissions for $CHBr_3$ and CH_2Br_2. The Ordóñez et al. (2012) inventory is also a top-down estimate based on the same set of aircraft measurements with the addition of the NASA POLARIS and SOLVE campaigns. This inventory weights tropical ($\pm20°$ latitude) $CHBr_3$ and CH_2Br_2 emissions according to a monthly-varying satellite climatology of chlorophyll a (chl a), a proxy for oceanic bio-productivity, providing some seasonality to the emission fluxes. The

155   Ziska et al. (2013) inventory is a bottom-up estimate of VSLS emissions, based on a compilation of seawater and ambient air measurements of $CHBr_3$ and CH_2Br_2. Climatological, aseasonal emission maps of these VSLS were calculated using the derived sea-air concentration gradients and a commonly used sea-to-air flux parameterisation; considering wind speed, sea surface temperature and salinity (Nightingale et al., 2000).

160 ## 2.2   Tropospheric chemistry

Participating models considered chemical loss of $CHBr_3$ and CH_2Br_2 through oxidation by the hydroxyl radical (OH) and by photolysis. These loss processes are comparable for $CHBr_3$, with photolysis contributing $\sim60\%$ of the $CHBr_3$ chemical sink at the surface (Hossaini et al., 2010). For CH_2Br_2, photolysis is a minor tropospheric sink, with its loss dominated by OH-initiated oxidation.

165   The overall local lifetimes of $CHBr_3$ and CH_2Br_2 in the tropical marine boundary layer have recently been evaluated to be 15 (13-17) and 94 (84-114) days, respectively (Carpenter and Reimann, 2014). These values are calculated based on [OH] = 1×10^6 molecules cm^{-3}, T = 275 K and with a global annual mean photolysis rate. For completeness, models also considered loss of $CHBr_3$ and CH_2Br_2 by reaction with atomic oxygen (O(^{1}D)) and chlorine (Cl) radicals. However, these are generally

170   very minor loss pathways owing to the far larger relative abundance of tropospheric OH and the respective rate constants for these reactions. Kinetic data (Table 1) was taken from the most recent Jet Propulsion Laboratory (JPL) data evaluation (Sander et al., 2011). Note, the focus and design of TransCom-VSLS was to constrain the stratospheric SGI of VSLS, thus product gases - formed following the breakdown of $CHBr_3$ and CH_2Br_2 in the TTL (Werner et al. 2016, in prep) - and the

175   stratospheric PGI of bromine was not considered.

    Participating models ran with the same global monthly-mean oxidant fields. For OH, O(^{1}D) and Cl, these fields were the same as those used in the previous TransCom-CH_4 model intercomparison (Patra et al., 2011). Within the TransCom framework, these fields have been exten-

sively used and evaluated and shown to give a realistic simulation of the tropospheric burden and lifetime of methane and also methyl chloroform. Models also ran with the same monthly-mean $CHBr_3$ and CH_2Br_2 photolysis rates, calculated offline from the TOMCAT chemical transport model (Chipperfield, 2006). TOMCAT has been used extensively to study the tropospheric chemistry of VSLS (e.g. Hossaini et al., 2010, 2012b, 2015b) and photolysis rates from the model were used to evaluate the lifetime of VSLS for the recent WMO Ozone Assessment Report (Carpenter and Reimann, 2014).

2.3 Participating models and output

Eight global models (ACTM, B3DCTM, EMAC, MOZART, NIES-TM, STAG, TOMCAT and UKCA) and 3 of their variants (see Table 2) participated in TransCom-VSLS. All the models are offline chemical transport models (CTMs), forced with analysed meteorology (e.g. winds and temperature fields), with the exception of EMAC and UKCA which are free-running chemistry-climate models (CCMs), calculating winds and temperature online. The horizontal resolution of models ranged from $\sim 1° \times 1°$ (longitude $\times$ latitude) to $3.75° \times 2.5°$. In the vertical, the number of levels varied from 32 to 85, with various coordinate systems. A summary of the models and their salient features is given in Table 2. Note, these features do not necessarily link to model performance as evaluated in this work. Note also, approximately half of the models used ECMWF ERA-Interim meteorological data. In terms of mean upwelling in the tropics, where stratospheric bromine SGI takes place, there is generally good agreement between the most recent major reanalysis products from ECMWF, JMA and NCEP (e.g. Harada et al., 2016). Therefore, we do not expect a particular bias in our results from use of ERA-Interim.

Three groups, the Karlsruhe Institute of Technology (KIT), the University of Leeds (UoL) and the University of Cambridge (UoC), submitted output from an additional set of simulations using variants of their models. KIT ran the EMAC model twice, as a free running model (here termed "EMAC_F") and also in *nudged* mode (EMAC_N). The UoL performed two TOMCAT simulations, the first of which used the model's *standard* convection parameterisation, based on the mass flux scheme of Tiedtke (1989). The second TOMCAT simulation ("TOMCAT_conv") used archived convective mass fluxes, taken from the ECMWF ERA-Interim reanalysis. A description and evaluation of these TOMCAT variants is given in Feng et al. (2011). In order to investigate the influence of resolution, the UoC ran two UKCA model simulations with different horizontal/vertical resolutions. The horizontal resolution in the "UKCA_high" simulation was a factor of 4 (2 in 2 dimensions) greater than that of the *standard* UKCA run (Table 2).

All participating models simulated the 6 $CHBr_3$ and CH_2Br_2 tracers (see Section 2.1) over a 20 year period; 01/01/1993 to 31/12/2012. This period was chosen as it (i) encompasses a range of field campaigns during which VSLS measurements were taken and (ii) allows the strong El Niño event of 1997/1998 to be investigated in the analysis of SGI trends. The monthly mean volume mixing ratio

(vmr) of each tracer was archived by each model on the same 17 pressure levels, extending from the surface to 10 hPa over the full simulation period. The models were also sampled hourly at 15 surface sites over the full simulation period and during periods of recent ship/aircraft measurement campaigns, described in Section 2.4 below. Note, the first two years of simulation were treated as spin up and output was analysed post 1995.

2.4 Observational data and processing

2.4.1 Surface

Model output was compared to and evaluated against a range of observational data. At the surface, VSLS measurements at 15 sites were considered (Table 3). All sites except one form part of the on-going global monitoring program (see http://www.esrl.noaa.gov/gmd) of the National Oceanic and Atmospheric Administration's Earth System Research Laboratory (NOAA/ESRL). Further details related to the sampling network are given in Montzka et al. (2011). Briefly, NOAA/ESRL measurements of $CHBr_3$ and CH_2Br_2 are obtained from whole air samples, collected approximately weekly into paired steel or glass flasks, prior to being analysed using gas chromatography/mass spectrometry (GC/MS) in their central Boulder laboratory. Here, the climatological monthly mean mole fractions of these VSLS were calculated at each site based on monthly mean surface measurements over the 01/01/98 to 31/12/2012 period (except SUM, THD and SPO which have shorter records). Similar climatological fields of $CHBr_3$, CH_2Br_2 were calculated from each model's hourly output sampled at each location.

Surface measurements of $CHBr_3$ and CH_2Br_2, obtained by the University of Cambridge in Malaysian Borneo (Tawau, site "TAW", Table 3), were also considered. A description of these data is given in Robinson et al. (2014). Briefly, in-situ measurements were made using the μ-Dirac gas chromatograph instrument with electron capture detection (GC-ECD) (e.g. Pyle et al., 2011). Measurements at TAW are for a single year (2009) only, making the observed record at this site far shorter than that at NOAA/ESRL stations discussed above.

A subset of models also provided hourly output over the period of the TransBrom and SHIVA (Stratospheric Ozone: Halogen Impacts in a Varying Atmosphere) ship cruises. During both campaigns, surface $CHBr_3$ and CH_2Br_2 measurements were obtained on-board the Research Vessel (R/V) *Sonne*. TransBrom sampled along a meridional transect of the West Pacific, from Japan to Australia, during October 2009 (Krüger and Quack, 2013). SHIVA was a European Union (EU)-funded project to investigate the emissions, chemistry and transport of VSLS (http://shiva.iup.uni-heidelberg.de/). Ship-borne measurements of surface $CHBr_3$ and CH_2Br_2 were obtained in November 2011, with sampling extending from Singapore to the Philippines, within the South China Sea and along the northern coast of Borneo (Fuhlbrügge et al., 2015). The ship track is shown in Figure 2.

2.4.2 Aircraft

Observations of $CHBr_3$ and CH_2Br_2 from a range of aircraft campaigns were also used (Figure 2). As (i) the troposphere-to-stratosphere transport of air (and VSLS) primarily occurs in the tropics, and (ii) because VSLS emitted in the extratropics have a negligible impact on stratospheric ozone (Tegtmeier et al., 2015), TransCom-VSLS focused on aircraft measurements obtained in the latitude range 30°N to 30°S. Hourly model output was interpolated to the relevant aircraft sampling location, allowing for point-by-point model-measurement comparisons. A brief description of the aircraft campaigns follows.

The HIAPER Pole-to-Pole Observations (HIPPO) project (http://www.eol.ucar.edu/projects/hippo) comprised a series of aircraft campaigns between 2009 and 2011 (Wofsy et al., 2011), supported by the National Science Foundation (NSF). Five campaigns were conducted; HIPPO-1 (January 2009), HIPPO-2 (November 2009), HIPPO-3 (March/April 2010), HIPPO-4 (June 2011) and HIPPO-5 (August/September 2011). Sampling spanned a range of latitudes, from near the North Pole to coastal Antarctica, on board the NSF Gulfstream V aircraft, and from the surface to ~14 km over the Pacific Basin. Whole air samples, collected in stainless steel and glass flasks, were analysed by two different laboratories using GC/MS; NOAA/ESRL and the University of Miami. HIPPO results from both laboratories are provided on a scale consistent with NOAA/ESRL.

The SHIVA aircraft campaign, based in Miri (Malaysian Borneo), was conducted during November—December 2011. Measurements of $CHBr_3$ and CH_2Br_2 were obtained during 14 flights of the DLR Falcon aircraft, with sampling over much of the northern coast of Borneo, within the South China and Sulu seas, up to an altitude of ~12 km (Sala et al., 2014; Fuhlbrügge et al., 2015). VSLS measurements were obtained by two groups; the University of Frankfurt (UoF) and the University of East Anglia (UEA). UoF measurements were made using an in-situ GC/MS system (Sala et al., 2014), while UEA analysed collected whole air samples, using GC/MS.

CAST (Coordinated Airborne Studies in the Tropics) is an ongoing research project funded by the UK Natural Environment Research Council (NERC) and is a collaborative initiative with the NASA ATTREX programme (see below). The CAST aircraft campaign, based in Guam, was conducted in January-February 2014 with VSLS measurements made by the University of York on-board the FAAM (Facility for Airborne Atmospheric Measurements) BAe-146 aircraft, up to an altitude of ~8 km. These observations were made by GC/MS collected from whole air samples as described in Andrews et al. (2016).

Observations of $CHBr_3$ and CH_2Br_2 within the TTL and lower stratosphere (up to ~20 km) were obtained during the NASA (i) Pre-Aura Validation Experiment (Pre-AVE), (ii) Costa Rica Aura Validation Experiment (CR-AVE) and (iii) Airborne Tropical TRopopause EXperiment (ATTREX) missions. The Pre-AVE mission was conducted in 2004 (January-February), with measurements obtained over the equatorial eastern Pacific during 8 flights of the high altitude WB-57 aircraft. The CR-AVE mission took place in 2006 (January-February) and sampled a similar region around

Costa Rica (Figure 2), also with the WB-57 aircraft (15 flights). The ATTREX mission consists of an ongoing series of aircraft campaigns using the unmanned Global Hawk aircraft. Here, $CHBr_3$ and CH_2Br_2 measurements from 10 flights of the Global Hawk, over two ATTREX campaigns, were used. The first campaign (February-March, 2013) sampled large stretches of the north east and central Pacific ocean, while the second campaign (January-March, 2014) sampled predominantly the West Pacific, around Guam. During Pre-AVE, CR-AVE and ATTREX, VSLS measurements were obtained by the University of Miami following GC/MS analysis of collected whole air samples.

3   Results and Discussion

3.1   Model-observation comparisons: surface

In this section, we evaluate the models in terms of (i) their ability to capture the observed seasonal cycle of $CHBr_3$ and CH_2Br_2 at the surface and (ii) the absolute agreement to the observations. We focus on investigating the relative performance of each of the tested emission inventories, within a given model, and the performance of the inventories across the ensemble.

3.1.1   Seasonality

We first consider the seasonal cycle of $CHBr_3$ and CH_2Br_2 at the locations given in Table 3. Figure 3 compares observed and simulated ($CHBr_3$_L tracer) monthly mean anomalies, calculated by subtracting the climatological monthly mean $CHBr_3$ surface mole fraction from the climatological annual mean (to focus on the seasonal variability). Based on photochemistry alone, in the northern hemisphere (NH) one would expect a $CHBr_3$ winter (Dec-Feb) maximum owing to a reduced chemical sink (e.g. slower photolysis rates and lower [OH]) and thereby a relatively longer $CHBr_3$ lifetime. This seasonality, apparent at most NH sites shown in Figure 3, is particularly pronounced at high-latitudes (>60°N, e.g. ALT, BRW and SUM), where the amplitude of the observed seasonal cycle is greatest. A number of features are apparent from these comparisons. First, in general most models reproduce the observed phase of the $CHBr_3$ seasonal cycle well, even with emissions that do not vary seasonally, suggesting that seasonal variations in the $CHBr_3$ chemical sink are generally well represented. For example, model-measurement correlation coefficients (r), summarised in Table 4, are >0.7 for at least 80% of the models at 7 of 11 NH sites. Second, at some sites, notably MHD, THD, CGO and PSA, the observed seasonal cycle of $CHBr_3$ is not captured well by virtually all of the models (see discussion below). Third, at most sites the amplitude of the seasonal cycle is generally consistent across the models (within a few percent, excluding clear outliers). The cause of outliers at a given site are likely in part related to the model sampling error, including distance of a model grid from the measurement site and resolution (as was shown for CO_2 in Patra et al. (2008)). These instances are rare for VSLS but can be seen in B3DCTM's output in Figure 3 for $CHBr_3$ at SMO. B3DCTM ran at a relatively coarse horizontal resolution (3.75°) and with less vertical layers

(40) compared to most other models. Note, it also has the simplest implementation of boundary layer mixing (Table 2). The above behaviour is also seen at SMO but to a lesser extent for CH_2Br_2, for which the seasonal cycle is smaller (see below). The STAG model also produces distinctly different features in the seasonal cycle of both species at some sites (prominently at CGO, SMO and HFM).

We attribute these deviations to STAG's parameterisation of boundary layer mixing, noting that differences for $CHBr_3$ are greater at KUM than at MLO – two sites in very close proximity but with the latter elevated at ∼3000 metres above sea level (i.e. above the boundary layer). With respect to the observations, the amplitude of the seasonal cycle is either under- (e.g. BRW) or over-estimated (e.g. KUM) at some locations, by all of the models. This possibly reflects a more systematic bias in the prescribed $CHBr_3$ loss rate and/or relates to emissions, though this effect is generally small and localised.

A similar analysis has been performed to examine the seasonal cycle of surface CH_2Br_2. Observed and simulated monthly mean anomalies, calculated in the same fashion as those for $CHBr_3$ above, are shown in Figure 4 and correlation coefficients are given in Table 5. The dominant chemical sink of CH_2Br_2 is through OH-initiated oxidation and thus its seasonal cycle at most stations reflects seasonal variation in [OH] and temperature. At most sites, this gives rise to a minimum in the surface mole fraction of CH_2Br_2 during summer months, owing to greater [OH] and temperature, and thereby a faster chemical sink. Relative to $CHBr_3$, CH_2Br_2 is considerably longer-lived (and thus well mixed) near the surface, meaning the amplitude of the seasonal cycle is far smaller. At most sites, most models capture the observed phase and amplitude of the CH_2Br_2 seasonal cycle well, though as was the case for $CHBr_3$, agreement in the southern hemisphere (SH, e.g. SMO, CGO, PSA) seems poorest. For example, at SMO and CGO only 40% of the models are positively correlated to the observations with $r > 0.5$ (Table 5). The NIES-TM model does not show major differences from other models for $CHBr_3$, but outliers for CH_2Cl_2 at SH sites (SMO to SPO) are apparent. We were unable to assign any specific reason for the inter-species differences seen for this model.

At two sites (MHD and THD) almost none of the models reproduce the observed $CHBr_3$ seasonal cycle, exhibiting an anti-correlation with the observed cycle (see bold entries in Table 4). Here, the simulated cycle follows that expected from seasonality in the chemical sink. At MHD, seasonality in the local emission flux is suggested to be the dominant factor controlling the seasonal cycle of surface $CHBr_3$ (Carpenter et al., 2005). This leads to the observed summer maximum (as shown in Figure 3) and is not represented in the models' $CHBr_3\_L$ tracer which, at the surface, is driven by the aseasonal emission inventory of Liang et al. (2010). A similar summer maximum seasonal cycle is observed for CH_2Br_2, also not captured by the models' $CH_2Br_2\_L$ tracer. To investigate the sensitivity of the model-measurement correlation to the prescribed surface fluxes, multi-model mean (MMM) surface $CHBr_3$ and CH_2Br_2 fields were calculated for each tracer (i.e. for each emission inventory considered) and each site. Figure 5 shows calculated MMM r values at each site for $CHBr_3$

and CH_2Br_2. For $CHBr_3$, r generally has a low sensitivity to the choice of emission fluxes at most sites (e.g. ALT, SUM, BRW, LEF, NWR, KUM, MLO, SPO), though notably at MHD, use of the Ziska et al. (2013) inventory (which is aseasonal) reverses the sign of r to give a strong positive correlation (MMM $r >0.70$) against the observations. Individual model r values for MHD are given in Table S1 of the Supplementary Information. With the exception of TOMCAT, TOMCAT_CONV and UKCA_HI, the remaining 7 models each reproduce the MHD $CHBr_3$ seasonality well (with $r >0.65$). That good agreement is obtained with the Ziska aseasonal inventory, compared to the other aseasonal inventories considered, highlights the importance of the $CHBr_3$ emission distribution, with respect to transport processes, serving this location. We suggest that the summertime transport of air that has experienced relatively large $CHBr_3$ emissions north/north-west of MHD is the cause of the apparent seasonal cycle seen in most models using the Ziska inventory (example animations of the seasonal evolution of surface $CHBr_3$ are given in the Supplementary Information to visualise this). Note also, the far better absolute model-measurement agreement obtained at MHD for models using this inventory (Supplementary Figure S3). At other sites, such as TAW, no clear seasonality is apparent in the observed background mixing ratios of $CHBr_3$ and CH_2Br_2 (Robinson et al., 2014). Here, the models exhibit little or no significant correlation to measured values and are unlikely to capture small-scale features in the emission distribution (e.g the contribution from local aquaculture) that conceivably contribute to observed levels of $CHBr_3$ and CH_2Br_2 in this region (Robinson et al., 2014).

3.1.2 Absolute agreement

To compare the absolute agreement between a model (M) and an observation (O) value, for each monthly mean surface model-measurement comparison, the mean absolute percentage error (MAPE, equation 1) was calculated for each model tracer. Figure 6 shows the $CHBr_3$ and CH_2Br_2 tracer that provides the lowest MAPE (i.e. best agreement) for each model (indicated by the fill colour of cells). The numbers within the cells give the MAPE value itself, and therefore correspond to the "best agreement" that can be obtained from the various tracers with the emission inventories that were tested.

$$\mathrm{MAPE} = \frac{100}{n} \sum_{t=1}^{n} |\frac{M_t - O_t}{O_t}| \tag{1}$$

For both $CHBr_3$ and CH_2Br_2, within any given model, no single emission inventory is able to provide the best agreement at all surface locations (i.e. from the columns in Figure 6). This was previously noted by Hossaini et al. (2013) using the TOMCAT model, and to some degree likely reflects the geographical coverage of the observations used to create the emission inventories. Hossaini et al. (2013) also noted significant differences between simulated and observed $CHBr_3$ and CH_2Br_2, using

the same inventory; i.e. at a given location, low $CHBr_3$ MAPE (good agreement) does not necessarily accompany a corresponding low CH_2Br_2 MAPE using the same inventory.

A key finding of this study is that significant inter-model differences are also apparent (i.e. see rows in Figure 6 grid). For example, for $CHBr_3$, no single inventory performs best across the full range of models at any given surface site. TOMCAT and B3DCTM - both of which are driven by ERA-Interim - agree on the best $CHBr_3$ inventory (lowest MAPE) at approximately half of the 17 sites considered. This analysis implies that, on a global scale, the "performance" of emission inventories is somewhat model-specific and highlights the challenges of evaluating such inventories. Previous conclusions as to the *best* performing VSLS inventories, based on single model simulations (Hossaini et al., 2013), must therefore be treated with caution. When one considers that previous modelling studies (Warwick et al., 2006; Liang et al., 2010; Ordóñez et al., 2012), each having derived different VSLS emissions based on aircraft observations, and having different tropospheric chemistry, report generally good agreement between their respective model and observations, our findings are perhaps not unexpected. However, we note also that few VSLS modelling studies have used long-term surface observations to evaluate their models, as performed here. This suggests any attempts to reconcile estimates of global VSLS emissions, obtained from different modelling studies, need to consider the influence of inter-model differences.

As the chemical sink of VSLS was consistent across all models, the inter-model differences discussed above are attributed primarily to differences in the treatment and implementation of transport processes. This includes convection and boundary layer mixing, both of which can significantly influence the near-surface abundance of VSLS in the real (Fuhlbrügge et al., 2013, 2015) and model (Zhang et al., 2008; Feng et al., 2011; Hoyle et al., 2011) atmospheres, and are parameterised in different ways (Table 2). On this basis, it is not surprising that different CTM setups lead to differences in the surface distribution of VSLS, nor that differences are apparent between CTMs that use the same meteorological input fields. Indeed, such effects have also been observed in previous model intercomparisons (Hoyle et al., 2011). Large-scale vertical advection, the native grid of a model and its horizontal/vertical resolution may also be contributing factors, though quantifying their relative influence was beyond the scope of TransCom-VSLS. At some sites, differences among emission inventory performance are apparent between model variants that, besides transport, are otherwise identical; i.e. TOMCAT and TOMCAT_CONV entries of Figure 6.

Despite the inter-model differences in the performance of emission inventories, some generally consistent features are found across the ensemble. First, for $CHBr_3$ the tropical MAPE (see Figure 7), based on the model-measurement comparisons in the latitude range $\pm20°$, is lowest when using the emission inventory of Ziska et al. (2013), for most (8 out of 11, $\sim70\%$) of the models. This is significant as troposphere-to-stratosphere transport primarily occurs in the tropics and the Ziska et al. (2013) inventory has the lowest $CHBr_3$ emission flux in this region (and globally, Table 1). Second, for CH_2Br_2, the tropical MAPE is lowest for most (also $\sim70\%$) of the models

when using the Liang et al. (2010) inventory, which also has the lowest global flux of the three inventories tested. For a number of models, a similar agreement is also obtained with Ordóñez et al. (2012) inventory, as the two are broadly similar in magnitude/distribution (Hossaini et al., 2013). For CH_2Br_2, the Ziska et al. (2013) inventory performs poorest across the ensemble (models generally overestimate CH_2Br_2 with this inventory). Overall, the tropical MAPE for a given model is more sensitive to choice of emission inventory for $CHBr_3$ than CH_2Br_2 (Figure 7). Based on each model's *preferred* inventory (i.e. from Figure 7), the tropical MAPE is generally ~40% for $CHBr_3$ and <20% for CH_2Br_2 (in most models). One model (STAG) exhibited a MAPE of >50% for both species, regardless of the choice of emission inventory, and was therefore omitted from the subsequent model-measurement comparisons to aircraft data and also from the multi-model mean SGI estimate derived in Section 3.5.

For the 5 models that submitted hourly output over the period of the SHIVA (2011) and TransBrom (2009) ship cruises, Figures 8 and 9 compare the multi-model mean (MMM) $CHBr_3$ and CH_2Br_2 mixing ratio (and the model spread) to the observed values. Note, the MMM was calculated based on each model's preferred tracer (i.e. preferred emissions inventory). Generally, the models reproduce the observed mixing ratios from SHIVA well, with a MMM campaign MAPE of 25% or less for both VSLS. This is encouraging as SHIVA sampled in the tropical West Pacific region, where rapid troposphere-to-stratosphere transport of VSLS likely occurs (e.g. Aschmann et al., 2009; Liang et al., 2014) and where VSLS emissions, weighted by their ozone depletion potential, are largest (Tegtmeier et al., 2015). Model-measurement comparisons during TransBrom are varied with models generally underestimating observed $CHBr_3$ and CH_2Br_2 during significant portions of the cruise. The underestimate is most pronounced close to the start and end of the cruise during which observed mixing ratios were more likely influenced by coastal emissions, potentially underestimated in global-scale models. Note, TransBrom also sampled sub-tropical latitudes (see Figure 2).

Overall, our results show that most models capture the observed seasonal cycle and the magnitude of surface $CHBr_3$ and CH_2Br_2 reasonably well, using a combination of emission inventories. Generally, this leads to a realistic surface distribution at most locations, and thereby provides good agreement between models and aircraft observations above the boundary layer; see Section 3.2 below.

3.2 Model-observation comparisons: free troposphere

We now evaluate modelled profiles of $CHBr_3$ and CH_2Br_2 using observations from a range of recent aircraft campaigns (see Section 2.4). Note, for these comparisons, and from herein unless noted, all analysis is performed using the *preferred* $CHBr_3$ and CH_2Br_2 tracer for each model (i.e. preferred emissions inventory), as was diagnosed in the previous discussion (i.e. from Figure 7, see also Section 3.1.2). This approach ensures that an estimate of stratospheric bromine SGI, from a given

model, is based on a simulation in which the optimal $CHBr_3$/CH_2Br_2 model-measurement agreement at the surface was acheived. The objective of the comparisons below is to show that the models produce a realistic simulation of $CHBr_3$ and CH_2Br_2 in the tropical free troposphere and to test model transport of $CHBr_3$ and CH_2Br_2 from the surface to high altitudes, against that from atmospheric measurements. Intricacies of individual model-measurement comparison are not discussed. Rather, Figure 10 compares MMM profiles (and the model spread) of $CHBr_3$ and CH_2Br_2 mixing ratio to observed campaign means within the tropics ($\pm 20°$ latitude). Generally model-measurement agreement, diagnosed by both the campaign-averaged MAPE and the correlation coefficient (r) is excellent during most campaigns. For all of the 7 campaigns considered, the modelled MAPE for $CHBr_3$ is $\leq 35\%$ ($\leq 20\%$ for CH_2Br_2). The models also capture much of the observed variability throughout the observed profiles, including, for example, the signature "c-shape" of convection in the measured $CHBr_3$ profile from SHIVA and HIPPO-1 (panel (a), 2nd and 3rd rows of Figure 10). Correlation coefficients between modelled and observed $CHBr_3$ are ≥ 0.8 for 5 of the 7 campaigns and for CH_2Br_2 are generally >0.5.

It is unclear why model-measurement agreement (particularly the $CHBr_3$ MAPE) is poorest for the HIPPO-4 and HIPPO-5 campaigns. However, we note that at most levels MMM $CHBr_3$ and CH_2Br_2 falls within ± 1 standard deviation (σ) of the observed mean. Note, an underestimate of surface $CHBr_3$ does not generally translate to a consistent underestimate of measured $CHBr_3$ at higher altitude. Critically, for the most part, the models are able to reproduce observed values of both gases well at ~ 12-14 km, within the lower TTL. Recall that the TTL is defined as the layer between the level of main convective outflow (~ 200 hPa, ~ 12 km) and the tropical tropopause (~ 100 hPa, ~ 17 km) (Gettelman and Forster, 2002). For a given model, simulations using the non-preferred tracers (i.e. with different $CHBr_3$/CH_2Br_2 emission inventories, not shown), generally lead to worse model-measurement agreement in the TTL. This is not surprising as model-measurement agreement at the surface is poorer in those simulations (as discussed in Section 3.1.2.).

Overall, given the large spatial/temporal variability in observed VSLS mixing ratios, in part due to the influence of transport processes, global-scale models driven by aseasonal emissions and using parameterised sub-grid scale transport schemes face challenges in reproducing VSLS observations in the tropical atmosphere. Yet despite this, we find that the TransCom-VSLS models generally provide a very good simulation of the tropospheric abundance of $CHBr_3$ and CH_2Br_2, particularly in the important tropical West Pacific region (e.g. SHIVA comparisons).

3.3 Model-observation comparisons: TTL and lower stratosphere

Figure 11 compares model profiles of $CHBr_3$ and CH_2Br_2 with high altitude measurements obtained in the TTL, extending into the tropical lower stratosphere. Across the ensemble, model-measurement agreement is varied but generally the models capture observed $CHBr_3$ from the Pre-AVE and CR-AVE campaigns, in the Eastern Pacific, well. It should be noted that the number of observations

500   varies significantly between these two campaigns; CR-AVE had almost twice the number of flights as Pre-AVE and this is reflected in the larger variability in the observed profile, particularly in the lower TTL. For both campaigns, the models capture the observed gradients in $CHBr_3$ and variability throughout the profiles; model-measurement correlation coefficients (r) for all of the models are >0.93 and >0.88 for Pre-AVE and CR-AVE, respectively. In terms of absolute agreement, 100% of

505   the models fall within $\pm 1\sigma$ of the observed $CHBr_3$ mean at the tropopause during Pre-AVE (and $\pm 2\sigma$ for CR-AVE). For both campaigns, virtually all models are within the measured (min-max) range (not shown) around the tropopause.

     During both ATTREX campaigns, larger $CHBr_3$ mixing ratios were observed in the TTL (panels c and d of Figure 11). This reflects the location of the ATTREX campaigns compared to Pre-AVE and

510   CR-AVE; over the tropical West Pacific, the level of main convective outflow extends deeper into the TTL compared to the East Pacific (Gettelman and Forster, 2002), allowing a larger portion of the surface $CHBr_3$ mixing ratio to detrain at higher altitudes. Overall, model-measurement agreement of $CHBr_3$ in the TTL is poorer during the ATTREX campaigns, with most models exhibiting a low bias between 14-16 km altitude. MOZART and UKCA simulations (which prefer the Liang $CHBr_3$

515   inventory) exhibit larger mixing ratios in the TTL, though are generally consistent with other models around the tropopause. Most ($\geq 70\%$) of the models reproduce $CHBr_3$ at the tropopause to within $\pm 1\sigma$ of the observed mean and all the models are within the measured range (not shown) during both ATTREX campaigns. Model-measurement $CHBr_3$ correlation is >0.8 for each ATTREX campaign, showing that again much of the observed variability throughout the $CHBr_3$ profiles is captured. The

520   same is true for CH_2Br_2, with $r > 0.84$ for all but one of the models during Pre-AVE and $r > 0.88$ for all of the models in each of the other campaigns.

     Overall, mean $CHBr_3$ and CH_2Br_2 mixing ratios around the tropopause, observed during the 2013/2014 ATTREX missions, are larger than the mean mixing ratios (from previous aircraft campaigns) reported in the latest WMO Ozone Assessment Report (Table 1-7 of Carpenter and Reimann

525   (2014)). As noted, this likely reflects the location at which the measurements were made; ATTREX 2013/2014 sampled in the tropical West and Central Pacific, whereas the WMO estimate is based on a compilation of measurements with a paucity in that region. From Figure 11, observed $CHBr_3$ and CH_2Br_2 at the tropopause was (on average) ∼0.35 ppt and ∼0.8 ppt, respectively, during ATTREX 2013/2014, compared to the 0.08 (0.00—0.31) ppt $CHBr_3$ and 0.52 (0.3-–0.86) ppt CH_2Br_2 ranges

530   reported by Carpenter and Reimann (2014).

3.4   Seasonal and zonal variations in the troposphere-to-stratosphere transport of VSLS

In this section we examine seasonal and zonal variability in the loading of $CHBr_3$ and CH_2Br_2 in the TTL and lower stratosphere, indicative of transport processes. In the tropics, a number of previous studies have shown a marked seasonality in convective outflow around the tropopause,

535   owing to seasonal variations in convective cloud top heights (e.g. Folkins et al., 2006; Hosking et al.,

2010; Bergman et al., 2012). Such variations influence the near-tropopause abundance of brominated VSLS (Hoyle et al., 2011; Liang et al., 2014) and other tracers, such as CO (Folkins et al., 2006).

Figures 12 and 13 show the simulated seasonal cycle of $CHBr_3$ and CH_2Br_2, respectively, at the base of the TTL and the cold point tropopause (CPT). $CHBr_3$ exhibits a pronounced seasonal cycle at the CPT, with virtually all models showing the same phase; with respect to the annual mean and integrated over the tropics, $CHBr_3$ is most elevated during boreal winter (DJF). The amplitude of the cycle varies considerably between models, with departures from the annual mean ranging from around $\pm10\%$ to $\pm40\%$, in a given month (panel b of Figure 12). Owing to its relatively long tropospheric lifetime, particularly in the TTL (>1 year) (Hossaini et al., 2010), CH_2Br_2 exhibits a weak seasonal cycle at the CPT as it is less influenced by seasonal variations in transport.

Panels (c) and (d) of Figures 12 and 13, also show the modelled absolute mixing ratios of $CHBr_3$ and CH_2Br_2 at the TTL base and CPT. Annually averaged, for $CHBr_3$, the model spread results in a factor of ~3 difference in simulated $CHBr_3$ at both levels (similarly, for CH_2Br_2 a factor of 1.5). The modelled mixing ratios fall within the measurement-derived range reported by Carpenter and Reimann (2014). The MMM $CHBr_3$ mixing ratio at the TTL base is 0.51 ppt, within the 0.2-1.1 ppt measurement-derived range. At the CPT, the MMM $CHBr_3$ mixing ratio is 0.20 ppt, also within the measured range of 0.0-0.31 ppt. On average, the models suggest a $\sim60\%$ gradient in $CHBr_3$ between the TTL base and tropopause. Similarly, the annual MMM CH_2Br_2 mixing ratio is 0.82 ppt at the TTL base, within the measured range of 0.6-1.2 ppt, and at the CPT is 0.73 ppt, within the measured range of 0.3-0.86 ppt. On average, the models show a CH_2Br_2 gradient of 10% between the two levels. These model absolute values are annual means over the whole tropical domain. However, zonal variability in VSLS loading within the TTL is expected to be large (e.g. Aschmann et al., 2009; Liang et al., 2014), owing to inhomogeneity in the spatial distribution of convection and oceanic emissions. The Indian Ocean, the Maritime Continent (incorporating Malaysia, Indonesia, and the surrounding islands and ocean), central America, and central Africa are all convectively-active regions, shown to experience particularly deep convective events with the potential, therefore, to rapidly loft VSLS from the surface into the TTL (e.g. Gettelman et al., 2002, 2009; Hosking et al., 2010). As previously noted, the absolute values can vary, though generally the TransCom-VSLS models agree on the locations with the highest VSLS mixing ratios, as seen from the zonal $CHBr_3$ anomalies at the CPT shown in Figure 14. These regions are consistent with the convective source regions discussed above. The largest $CHBr_3$ mixing ratios at the CPT are predicted over the tropical West Pacific ($20°S$-$20°N$, $100°E$-$180°E$), particularly during DJF. Integrated over the tropical domain, this signal exerts the largest influence on the $CHBr_3$ seasonal cycle at the CPT. This result is consistent with the model intercomparison of Hoyle et al. (2011), who examined the seasonal cycle of idealised VSLS-like tracers around the tropopause, and reported a similar seasonality.

While meridionally, the width of elevated $CHBr_3$ mixing ratios during DJF is similar across the models, differences during boreal summer (JJA) are apparent, particularly in the vicinity of the Asian

Monsoon (5°N-35°N, 60°E-120°E). Note, the CHBr$_3$ anomalies shown in Figure 14 correspond to departures from the mean calculated in the latitude range of $\pm 30°$, and therefore encompass most of the Monsoon region. A number of studies have highlighted (i) the role of the Monsoon in transporting pollution from east Asia into the stratosphere (e.g. Randel et al., 2010) and (ii) its potential role in the troposphere-to-stratosphere transport of aerosol precursors, such as volcanic SO$_2$ (e.g. Bourassa et al., 2012; Fromm et al., 2014). For VSLS, and other short-lived tracers, the Monsoon may also represent a significant pathway for transport to the stratosphere (e.g. Vogel et al., 2014; Orbe et al., 2015; Tissier and Legras , 2016). Here, a number of models show elevated CHBr$_3$ in the lower stratosphere over the Monsoon region, though the importance of the Monsoon with respect to the tropics as a whole varies substantially between the models. For example, from Figure 14, models such as ACTM and UKCA show far greater enhancement in CHBr$_3$ associated with the Monsoon during JJA, compared to others (e.g. MOZART, TOMCAT). A comparison of CHBr$_3$ anomalies at 100 hPa but confined to the Monsoon region, as shown in Figure 15, reveals a Monsoon signal in most of the models, but as noted above the strength of this signal varies considerably. The STAG model, which does not include a treatment of *deep* convection and has been shown to have weak ventilation through the boundary layer (Law et al., 2008), exhibits virtually no CHBr$_3$ enhancement over the Monsoon region.

The high altitude model-model differences in CHBr$_3$, highlighted in Figures 14 and 15, are attributed predominately to differences in the treatment of convection. Previous studies have shown that (i) convective updraft mass fluxes, including the vertical extent of deep convection (relevant for bromine SGI from VSLS), vary significantly depending on the implementation of convection in a given model (e.g. Feng et al., 2011) and (ii) that significantly different short-lived tracer distributions are predicted from different models using different convective parameterisations (e.g. Hoyle et al., 2011). Such parameterisations are often complex, relying on assumptions regarding detrainment levels, trigger thresholds for shallow, mid-level and/or deep convection, and vary in their approach to computing updraft (and downdraft) mass fluxes. Furthermore, the vertical transport of model tracers is also sensitive to interactions of the convective parameterisation with the boundary layer mixing scheme (also parameterised) (Rybka and Tost, 2014). On the above basis and considering that the TransCom-VSLS models implement these processes in different ways (Table 2), it was not possible to disentangle transport effects within the scope of this project. However, no systematic similarities/differences between models according to input meteorology were apparent. Examining the difference between UKCA_HI and UKCA_LO reveals that horizontal resolution is a significant factor. The UKCA_HI simulation shows a greater role of the Monsoon region, likely due to differences in the distribution of surface emissions (e.g. along longer coastlines in the higher resolution model) with respect to the occurrence of convection, as shown by Russo et al. (2015). Overall, aircraft VSLS observations within this poorly sampled region are required in order to elucidate further the role of the Monsoon in the troposphere-to-stratosphere transport of brominated VSLS.

3.5 Stratospheric source gas injection of bromine and trends

In this section we quantify the climatological SGI of bromine from $CHBr_3$ and CH_2Br_2 to the tropical LS and examine inter-annual variability. The current measurement-derived range of bromine SGI ($[3 \times CHBr_3] + [2 \times CH_2Br_2]$ at the tropical tropopause) from these two VSLS is 1.28 (0.6-2.65) ppt Br, i.e. uncertain by a factor of $\sim$4.5 (Carpenter and Reimann, 2014). This uncertainty dominates the overall uncertainty on the *total* stratospheric bromine SGI range (0.7-3.4 ppt Br), which includes relatively minor contributions from other VSLS (e.g. $CHBr_2Cl$, CH_2BrCl and $CHBrCl_2$). Given that SGI may account for up to 76% of stratospheric Br_y^{VSLS} (Carpenter and Reimann, 2014) (note, Br_y^{VSLS} also includes the contribution of product gas injection), constraining the contribution from $CHBr_3$ and CH_2Br_2 is, therefore, desirable.

The TransCom-VSLS climatological MMM estimate of Br SGI from $CHBr_3$ and CH_2Br_2 is 2.0 (1.2-2.5) ppt Br, with the reported uncertainty from the model spread. CH_2Br_2 accounts for $\sim$72% of this total, in good agreement with the $\sim$80% reported by Carpenter and Reimann (2014). The model spread encompasses the best estimate reported by Carpenter and Reimann (2014), though our best estimate is 0.72 ppt (57%) larger. The spread in the TransCom-VSLS models is also 37% lower than the Carpenter and Reimann (2014) range, suggesting that their measurement-derived range in bromine SGI from $CHBr_3$ and CH_2Br_2 is possibly too conservative, particularly at the lower limit (Figure 16), and from a climatological perspective. We note that (i) the TransCom-VSLS estimate is based on models, shown here, to simulate the surface to tropopause abundance of $CHBr_3$ and CH_2Br_2 well and (ii) represents a climatological estimate over the simulation period, 1995-2012. The measurement-derived best estimate and range (i.e. that from Carpenter and Reimann (2014)) does not include the high altitude observations over the tropical West Pacific obtained during the most recent NASA ATTREX missions. As noted in Section 3.3, mean $CHBr_3$ and CH_2Br_2 measured around the tropopause during ATTREX (2013/2014 missions), is at the upper end of the compilation of observed values given in the recent WMO Ozone Assessment Report (Table 1-7 of Carpenter and Reimann (2014)). Inclusion of these data would bring the WMO SGI estimate from $CHBr_3$ and CH_2Br_2 closer to the TransCom-VSLS estimate reported here. For context, the TransCom-VSLS MMM estimate of Br SGI from $CHBr_3$ and CH_2Br_2 (2.0 ppt Br) represents 10% of *total* stratospheric Br_y (i.e. considering long-lived sources gases also) - estimated at $\sim$20 ppt in 2011 (Carpenter and Reimann, 2014).

The TransCom-VSLS MMM SGI range discussed above is from $CHBr_3$ and CH_2Br_2 only. *Minor* VSLS, including $CHBr_2Cl$, CH_2BrCl, $CHBrCl_2$, C_2H_5Br, C_2H_4Br and C_3H_7Br, are estimated to contribute a further 0.08 to 0.71 ppt Br through SGI (Carpenter and Reimann, 2014). If we add this contribution on to our MMM estimate of bromine SGI from $CHBr_3$ and CH_2Br_2, a reasonable estimate of 1.28 to 3.21 ppt Br is derived from our results for the *total* SGI range. This range is 28% smaller than the equivalent estimate of total SGI reported by Carpenter and Reimann (2014), because of the constraint on the contribution from $CHBr_3$ and CH_2Br_2, as discussed above.

Our uncertainty estimate on simulated bromine SGI (from the model spread) reflects inter-model variability, primarily due to differences in transport, but does not account for uncertainty on the chemical factors influencing the loss rate and lifetime of VSLS (e.g. tropospheric [OH]) - as all of the models used the same prescribed oxidants. However, Aschmann and Sinnhuber (2013) found that the stratospheric SGI of Br exhibited a low sensitivity to large perturbations to the chemical loss rate of $CHBr_3$ and CH_2Br_2; a $\pm 50\%$ perturbation to the loss rate changed bromine SGI by 2% at most in their model sensitivity experiments. Furthermore, our SGI range is compatible with recent model SGI estimates that used different [OH] fields; for example, Fernandez et al. (2014) simulated a stratospheric SGI of 1.7 ppt Br from $CHBr_3$ and CH_2Br_2.

We found no clear long-term transport-driven trend in the stratospheric SGI of bromine. Clearly, this result is limited to the study period examined and does not preclude potential future changes due to climate change, as suggested by some studies (e.g. Hossaini et al., 2012b). In terms of inter-annual variability, the simulated annual mean bromine SGI varied by $\pm 5\%$ around the climatological mean (panel (b) of Figure 16) over the simulation period (small in the context of total stratospheric Br_y, see above). Naturally, this encompasses inter-annual variability of both $CHBr_3$ and CH_2Br_2 reaching the tropical LS. The latter of which is far smaller and given that CH_2Br_2 is the larger contributor to SGI, dampens the overall inter-annual variability. Note, inter-annual changes in emissions, [OH] or photolysis rates were not quantified here (only transport). On a monthly basis, the amount of $CHBr_3$ reaching the tropical LS can clearly exhibit larger variability. $CHBr_3$ anomalies (calculated as monthly departures from the climatological monthly mean mixing ratio) at the tropical tropopause are shown in Figure 17. Also shown in Figure 17 is the Multivariate ENSO Index (MEI) - a time-series which characterises ENSO intensity based on a range of meteorological and oceanographic components (Wolter and Timlin, 1998). See also: http://www.esrl.noaa.gov/psd/enso/mei/. The transport of $CHBr_3$ (and CH_2Br_2, not shown) to the tropical LS is strongly correlated (r values ranging from 0.6 to 0.75 across the ensemble) to ENSO activity over the Eastern Pacific (owing to the influence of sea surface temperature on convection). For example, a clear signal of the very strong El Niño event of 1997/1998 is apparent in the models (i.e. with enhanced $CHBr_3$ at the tropopause) supporting the notion that bromine SGI is sensitive to such climate modes, in *this* region (Aschmann et al., 2011). However, when averaged over the tropics no strong correlation between VSLS loading in the LS and the MEI (or just sea surface temperature) was found across the ensemble. We suggest that zonal variations in SST anomalies (and convective activity) associated with ENSO, with warming in some regions and cooling in others, has a cancelling effect on the tropical mean bromine SGI. Indeed, previous model studies have showed a marked zonal structure in $CHBr_3/CH_2Br_2$ loading in the LS in strong ENSO years, with relative increases and decreases with respect to climatological averages depending on region (Aschmann et al., 2011). Further investigation, beyond the scope of this work, is needed to determine the sensitivity of *total* stratospheric

$\mathrm{Br}_y^{\mathrm{VSLS}}$ (i.e. including the contribution from product gas injection), to this and other modes of climate variability.

4 Summary and Conclusions

Understanding the chemical and dynamical processes which influence the atmospheric loading of VSLS in the present, and how these processes may change in the future, is important to understand the role of VSLS in a number of issues. In the context of the stratosphere, it is important to (i) determine the relevance of VSLS for assessments of O_3 layer recovery timescales (Yang et al., 2014), (ii) assess the full impact of proposed stratospheric geoengineering strategies (Tilmes et al., 2012) and (iii) accurately quantify the ozone-driven radiative forcing (RF) of climate (Hossaini et al., 2015a). Here we performed the first concerted multi-model intercomparison of halogenated VSLS. The overarching objective of TransCom-VSLS was to provide a reconciled model estimate of the SGI of bromine from $CHBr_3$ and CH_2Br_2 to the lower stratosphere and to investigate inter-model differences due to emissions and transport processes. Participating models performed simulations over a 20-year period, using a standardised chemistry setup (prescribed oxidants/photolysis rates) to isolate, predominantly, transport-driven variability between models. We examined the sensitivity of results to the choice of $CHBr_3$/CH_2Br_2 emission inventory within individual models, and also quantified the performance of emission inventories across the ensemble. The main findings of TransCom-VSLS are summarised below.

– The TransCom-VSLS models reproduce the observed surface abundance, distribution and seasonal cycle of $CHBr_3$ and CH_2Br_2, at most locations where long-term measurements are available, reasonably well. At most sites, (i) the simulated seasonal cycle of these VSLS is not particularly sensitive to the choice of emission inventory, and (ii) the observed cycle is reproduced well simply from seasonality in the chemical loss (a notable exception is at Mace Head, Ireland). Within a given model, absolute model-measurement agreement at the surface is highly dependent on the choice of VSLS emission inventory, particularly for $CHBr_3$ for which the global emission distribution and magnitude is somewhat poorly constrained. We find that at a number of locations, no consensus among models as to which emission inventory performs best can be reached. This is due to differences in the representation/implementation of transport processes between models which can significantly influence the boundary layer abundance of short-lived tracers. This effect was observed between CTM variants which, other than tropospheric transport schemes, are identical. A major implication of this finding is that care must be taken when assessing the performance of emission inventories in order to constrain global VSLS emissions, based on single model studies alone. However, we also find that within the tropics - where the troposphere-to-stratosphere transport of VSLS takes place - most models ($\sim$70%) achieve best agreement with measured surface $CHBr_3$ when using a bottom-up derived inventory, with the lowest $CHBr_3$ emission flux (Ziska et al., 2013). Similarly for CH_2Br_2 most

(also $\sim$70%) of the models achieve optimal agreement using the CH_2Br_2 inventory with the lowest tropical emissions (Liang et al., 2010), though agreement is generally less sensitive to the choice of emission inventory (compared to $CHBr_3$). Recent studies have questioned the effectiveness of us-ing aircraft observations and global-scale models (i.e. the top-down approach) in order to constrain regional VSLS emissions (Russo et al., 2015). For this reason and given growing interest as to pos-sible climate-driven changes in VSLS emissions (e.g. Hughes et al., 2012), online calculations (e.g. Lennartz et al., 2015) which (i) consider interactions between the ocean/atmosphere state (based on observed seawater concentrations) and (ii) produce seasonally-resolved sea-to-air fluxes may prove a more insightful approach, over use of prescribed emission climatologies, in future modelling work.

– The TransCom-VSLS models generally agree on the locations where $CHBr_3$ and CH_2Br_2 are most elevated around the tropopause. These locations are consistent with known convectively active re-gions and include the Indian Ocean, the Maritime Continent and wider tropical West Pacific and the tropical Eastern Pacific, in agreement with of a number of previous VSLS-focused modelling studies (e.g. Aschmann et al., 2009; Pisso et al., 2010; Hossaini et al., 2012b; Liang et al., 2014). Owing to significant inter-model differences in transport processes, both the absolute tracer amount transported to the stratosphere and the amplitude of the seasonal cycle varies among models. How-ever, of the above regions, the tropical West Pacific is the most important in all of the models (re-gardless of the emission inventory), due to rapid vertical ascent of VSLS simulated during boreal winter. In the free troposphere, the models reproduce observed $CHBr_3$ and CH_2Br_2 from the re-cent SHIVA and CAST campaigns in this region to within $\leq$16% and $\leq$32%, respectively. How-ever, at higher altitudes in the TTL the models generally (i) underestimated $CHBr_3$ between 14-16 km observed during the 2014 NASA ATTREX mission in this region but (ii) fell within ±1 σ of the observed mean around the tropical tropopause ($\sim$17 km). Generally good agreement was also obtained to high altitude aircraft measurements of VSLS around the tropopause in the Eastern Pa-cific. During boreal summer, most models show elevated $CHBr_3$ around the tropopause above the Asian Monsoon region. However, the strength of this signal varies considerably among the mod-els with a spread that encompasses virtually no $CHBr_3$ enhancement over the Monsoon region to strong (85%) $CHBr_3$ enhancements at the tropopause, with respect to the zonal average. Measure-ments of VSLS in the poorly sampled Monsoon region from the upcoming StratoClim campaign (http://www.stratoclim.org/) will prove useful in determining the importance of this region for the troposphere-to-stratosphere transport of VSLS.

– Climatologically, we estimate that $CHBr_3$ and CH_2Br_2 contribute 2.0 (1.2-2.5) ppt Br to the lower stratosphere through SGI, with the reported uncertainty due to the model spread. The TransCom-VSLS best estimate of 2.0 ppt Br is (i) $\sim$57% larger than the measurement-derived best estimate of 1.28 ppt Br reported by Carpenter and Reimann (2014), and (ii) the TransCom-VSLS range (1.2-2.5 ppt Br) is $\sim$37% smaller than the 0.6-2.65 ppt Br range reported by Carpenter and Reimann (2014). From this we suggest that, climatologically, the Carpenter and Reimann (2014) measurement-derived

755 SGI range, based on a limited number of aircraft observations (with a particular paucity in the tropical West Pacific), is potentially too conservative at the lower limit. Although we acknowledge that our uncertainty estimate (the model spread) does not account for a number of intrinsic uncertainties within global models, for example, tropospheric [OH] (as the models used the same set of prescribed oxidants). No significant transport-driven trend in stratospheric bromine SGI was found over the sim-

760 ulation period, though inter-annual variability was of the order of $\pm 5\%$. Loading of both CHBr$_3$ and CH$_2$Br$_2$ around the tropopause over the East Pacific is strongly coupled to ENSO activity but no strong correlation to ENSO or sea surface temperature was found when averaged across the wider tropical domain.

Overall, results from the TransCom-VSLS model intercomparison support the large body of evidence that natural VSLS contribute significantly to stratospheric bromine. Given suggestions that

765 VSLS emissions from the growing aquaculture sector will likely increase in the future (WMO, 2014; Phang et al., 2015) and that climate-driven changes to ocean emissions (Tegtmeier et al., 2015), tropospheric transport and/or oxidising capacity (Dessens et al., 2009; Hossaini et al., 2012a) could lead to an increase in the stratospheric loading of VSLS, it is paramount to constrain the present

770 day Br$_y^{VSLS}$ contribution to allow any possible future trends to be determined. In addition to SGI, this will require constraint on the stratospheric product gas injection of bromine which conceptually presents a number of challenges for global models given its inherent complexity.

Acknowledgements. RH thanks M. Chipperfield for comments and the Natural Environment Research Council (NERC) for funding through the TropHAL project (NE/J02449X/1). PKP was supported by JSPS/MEXT

775 KAKENHI-A (grant 22241008). GK, B-MS and PK acknowledge funding by the Deutsche Forschungsgemeinschaft (DFG) through the Research Unit SHARP (SI 1400/1-2 and PF 384/9-1 and in addition through grant PF 384/12-1) and by the Helmholtz Association through the Research Programme ATMO. NRPH and JAP acknowledge support of this work through the ERC ACCI project (project no. 267760), and by NERC through grant nos. NE/J006246/1 and NE/F1016012/1. NRPH was supported by a NERC Advanced Research Fellow-

780 ship (NE/G014655/1). PTG was also support through ERC ACCI. Contribution of JA and R Hommel has been funded in part by the DFG Research Unit 1095 SHARP, and by the German Ministry of Education and Research (BMBF) within the project ROMIC-ROSA (grant 01LG1212A).

References

Andrews, S. J., Carpenter, L. J., Apel, E. C., Atlas, E., Donets, V., Hopkins, J. F., Hornbrook, R. S., Lewis, A. C., Lidster, R. T., Lueb, R., Minaeian, J., Navarro, M., Punjabi, S., Riemer, D., and Schauffler, S.: A comparison of very short-lived halocarbon (VSLS) and DMS aircraft measurements in the Tropical West Pacific from CAST, ATTREX and CONTRAST, Atmos. Meas. Tech. Discuss., doi:10.5194/amt-2016-94, in review, 2016.

Arakawa, A. and Shubert, W. H.: Interaction of a cumulus ensemble with the large-scale environment, Part I, J. Atmos. Sci., 31, 674– 704, 1974.

Archer, S. D., Goldson, L. E., Liddicoat, M. I., Cummings, D. G., and Nightingale, P. D.: Marked seasonality in the concentrations and sea-to-air flux of volatile iodocarbon compounds in the western English Channel, J. Geophys. Res., 112, C08009, doi:10.1029/2006JC003963, 2007.

Aschmann, J. and Sinnhuber, B.-M.: Contribution of very short-lived substances to stratospheric bromine loading: uncertainties and constraints, Atmos. Chem. Phys., 13, 1203–1219, doi:10.5194/acp-13-1203-2013, 2013.

Aschmann, J., Sinnhuber, B.-M., Atlas, E. L., and Schauffler, S. M.: Modeling the transport of very short-lived substances into the tropical upper troposphere and lower stratosphere, Atmos. Chem. Phys., 9, 9237–9247, 2009.

Aschmann, J., Sinnhuber, B.-M., Chipperfield, M. P., and Hossaini, R.: Impact of deep convection and dehydration on bromine loading in the upper troposphere and lower stratosphere, Atmos. Chem. Phys., 11, 2671–2687, doi:10.5194/acp-11-2671-2011, 2011.

Aschmann, J., Burrows, J. P., Gebhardt, C., Rozanov, A., Hommel, R., Weber, M., and Thompson, A. M.: On the hiatus in the acceleration of tropical upwelling since the beginning of the 21st century, Atmos. Chem. Phys., 14, 12803–12814, doi:10.5194/acp-14-12803-2014, 2014.

Ashfold, M. J., Harris, N. R. P., Manning, A. J., Robinson, A. D., Warwick, N. J., and Pyle, J. A.: Estimates of tropical bromoform emissions using an inversion method, Atmos. Chem. Phys., 14, 979–994, doi:10.5194/acp-14-979-2014, 2014.

Belikov, D., Maksyutov, S., Miyasaka, T., Saeki, T., Zhuravlev, R., and Kiryushov, B.: Mass-conserving tracer transport modelling on a reduced latitude-longitude grid with NIES-TM, Geosci. Model Dev., 4, 207–222, doi:10.5194/gmd-4-207-2011, 2011.

Belikov, D. A., Maksyutov, S., Sherlock, V., Aoki, S., Deutscher, N. M., Dohe, S., Griffith, D., Kyro, E., Morino, I., Nakazawa, T., Notholt, J., Rettinger, M., Schneider, M., Sussmann, R., Toon, G. C., Wennberg, P. O., and Wunch, D.: Simulations of column-averaged CO_2 and CH_4 using the NIES TM with a hybrid sigma-isentropic (σ–θ) vertical coordinate, Atmos. Chem. Phys., 13, 1713–1732, doi:10.5194/acp-13-1713-2013, 2013.

Bergman, J. W., Jensen, E. J., Pfister, L., and Yang, Q.: Seasonal differences of vertical-transport efficiency in the tropical tropopause layer: On the interplay between tropical deep convection, large-scale vertical ascent, and horizontal circulations, J. Geophys. Res., 117, D05302, doi:10.1029/2011JD016992, 2012.

Bourassa, A. E., Robock, A., Randel, W. J., Deshler, T., Rieger, L. A., Lloyd, N. D., Llewellyn, E. J. T., and Degenstein, D. A.: Large volcanic aerosol load in the stratosphere linked to asian monsoon transport, Science, 337, 78–81, doi:10.1126/science.1219371, 2012.

Brinckmann, S., Engel, A., Bönisch, H., Quack, B., and Atlas, E.: Short-lived brominated hydrocarbons – observations in the source regions and the tropical tropopause layer, Atmos. Chem. Phys., 12, 1213–1228, doi:10.5194/acp-12-1213-2012, 2012.

Carpenter, L. and Liss, P.: On temperate sources of bromoform and other reactive organic bromine gases, J. Geophys. Res., 105, 20 539–20 547, doi:10.1029/2000JD900242, 2000.

Carpenter, L., Wevill, D., O'Doherty, S., Spain, G., and Simmonds, P.: Atmospheric bromoform at Mace Head, Ireland: seasonality and evidence for a peatland source, Atmos. Chem. Phys., 5, 2927–2934, 2005.

Carpenter, L. J, Reimann, S, Burkholder, J. B., Clerbaux, C., Hall, B. D., Hossaini, R., Laube, J. C., and Yvon-Lewis, S. A.: Ozone-Depleting Substances (ODSs) and Other Gases of Interest to the Montreal Protocol, in: Scientific Assessment of Ozone Depletion: 2014, Global Ozone Research and Monitoring Project, Report No. 55, Chapt. 1, World Meteorological Organization, Geneva , 2014.

Chipperfield, M. P.: New version of the TOMCAT/SLIMCAT off-line chemical transport model: intercomparison of stratospheric tracer experiments, Q. J. Roy. Meteor. Soc., 132, 1179–1203, doi:10.1256/qj.05.51, 2006.

Chipperfield, M.: Nitrous oxide delays ozone recovery, Nat. Geosci., 2, 742–743, doi:10.1038/ngeo678, 2009.

Denning, A. S., Holzer, M., Gurney, K. R., Heimann, M., Law, R. M., Rayner, P. J., Fung, I. Y., Fan, S.-M., Taguchi, S., Freidlingstein, P., Balkanski, Y., Taylor, J., Maiss, M., and Levin, I.: Three-dimensional transport and concentration of SF6: A model intercomparison study (TransCom 2), Tellus, 51B, 266–297, 1999.

Dessens, O., Zeng, G., Warwick, N., and Pyle, J.: Short-lived bromine compounds in the lower stratosphere; impact of climate change on ozone, Atmos. Sci. Lett., 10, 201–206, doi:10.1002/asl.236, 2009.

Dorf, M., Butz, A., Camy-Peyret, C., Chipperfield, M. P., Kritten, L., and Pfeilsticker, K.: Bromine in the tropical troposphere and stratosphere as derived from balloon-borne BrO observations, Atmos. Chem. Phys., 8, 7265–7271, 2008.

Emmons, L. K., Walters, S., Hess, P. G., Lamarque, J.-F., Pfister, G. G., Fillmore, D., Granier, C., Guenther, A., Kinnison, D., Laepple, T., Orlando, J., Tie, X., Tyndall, G., Wiedinmyer, C., Baughcum, S. L., and Kloster, S.: Description and evaluation of the Model for Ozone and Related chemical Tracers, version 4 (MOZART-4), Geosci. Model Dev., 3, 43–67, doi:10.5194/gmd-3-43-2010, 2010.

Feng, W., Chipperfield, M. P., Dorf, M., Pfeilsticker, K., and Ricaud, P.: Mid-latitude ozone changes: studies with a 3-D CTM forced by ERA-40 analyses, Atmos. Chem. Phys., 7, 2357–2369, 2007.

Feng, W., Chipperfield, M. P., Dhomse, S., Monge-Sanz, B. M., Yang, X., Zhang, K., and Ramonet, M.: Evaluation of cloud convection and tracer transport in a three-dimensional chemical transport model, Atmos. Chem. Phys., 11, 5783–5803, doi:10.5194/acp-11-5783-2011, 2011.

Fernandez, R. P., Salawitch, R. J., Kinnison, D. E., Lamarque, J.-F., and Saiz-Lopez, A.: Bromine partitioning in the tropical tropopause layer: implications for stratospheric injection, Atmos. Chem. Phys., 14, 13 391–13 410, doi:10.5194/acp-14-13391-2014, 2014.

Folkins, I., Bernath, P., Boone, C., Lesins, G., Livesey, N., Thompson, A. M., Walker, K., and Witte, J. C.: Seasonal cycles of O_3, CO, and convective outflow at the tropical tropopause, Geophys. Res. Lett., 33, doi:10.1029/2006GL026602, 2006.

Forster, P. M. and Shine, K. P.: Radiative forcing and temperature trends from stratospheric ozone changes, J. Geophys. Res., 102, 10841-10855, doi:10.1029/96JD03510, 1997.

Fromm, M., Kablick, G., Nedoluha, G., Carboni, E., Grainger, R., Campbell, J., and Lewis, J.: Correcting the record of volcanic stratospheric aerosol impact: Nabro and Sarychev Peak, J. Geophys. Res., 119, 10,343—10,364, doi:10.1002/2014JD021507, 2014.

Fuhlbrügge, S., Krüger, K., Quack, B., Atlas, E., Hepach, H., and Ziska, F.: Impact of the marine atmospheric boundary layer conditions on VSLS abundances in the eastern tropical and subtropical North Atlantic Ocean, Atmos. Chem. Phys., 13, 6345–6357, doi:10.5194/acp-13-6345-2013, 2013.

Fuhlbrügge, S., Quack, B., Tegtmeier, S., Atlas, E., Hepach, H., Shi, Q., Raimund, S., and Krüger, K.: The contribution of oceanic halocarbons to marine and free troposphere air over the tropical West Pacific, Atmos. Chem. Phys. Discuss., 15, 17 887–17 943, doi:10.5194/acpd-15-17887-2015, 2015.

Gregory, D. and Rowntree, P. R.: A mass flux convection scheme with representation of cloud ensemble characteristics and stability-dependent closure, Mon. Weather Rev., 118, 1483– 1506, 1990.

Gettelman, A. and Forster, P. M.: A Climatology of the Tropical Tropopause Layer, J. Meteor. Soc. Japan., 80, 911–924, 2002.

Gettelman, A., Seidel, D. J., Wheeler, M. C., and Ross, R. J.: Multidecadal trends in tropical convective available potential energy, J. Geophys. Res., 107, 4606, doi:10.1029/2001JD001082, 2002.

Gettelman, A., Lauritzen, P. H., Park, M., and Kay, J. E.: Processes regulating short-lived species in the tropical tropopause layer, J. Geophys. Res., 114, doi:10.1029/2009JD011785, 2009.

Hack, J. J.: Parameterization of moist convection in the NCAR community climate model (CCM2), J. Geophys. Res., 99, 5551— 5568, 1994.

Harada, Y., Kamahori, H., Kobayashi, C., Endo, H., Kobayashi, S., Ota, Y., Onoda, H., Onogi, K., Miyaoka, K., and Takahashi, K.: The JRA-55 Reanalysis: Representation of atmospheric circulation and climate variability, J. Meteor. Soc. Japan, in press, 2016.

Holtslag, A. and Boville, B.: Local versus nonlocal boundary-layer diffusion in a global climate model, Journal of Climate, 6, 1825–1842, 1993.

Hosking, J. S., Russo, M. R., Braesicke, P., and Pyle, J. A.: Modelling deep convection and its impacts on the tropical tropopause layer, Atmos. Chem. Phys., 10, 11 175–11 188, doi:10.5194/acp-10-11175-2010, 2010.

Hossaini, R., Chipperfield, M. P., Monge-Sanz, B. M., Richards, N. A. D., Atlas, E., and Blake, D. R.: Bromoform and dibromomethane in the tropics: a 3-D model study of chemistry and transport, Atmos. Chem. Phys., 10, 719–735, doi:10.5194/acp-10-719-2010, 2010.

Hossaini, R., Chipperfield, M. P., Dhomse, S., Ordonez, C., Saiz-Lopez, A., Abraham, N. L., Archibald, A., Braesicke, P., Telford, P., Warwick, N., Yang, X., and Pyle, J.: Modelling future changes to the stratospheric source gas injection of biogenic bromocarbons, Geophys. Res. Let., 39, L20813, doi:10.1029/2012GL053401, 2012a.

Hossaini, R., Chipperfield, M. P., Feng, W., Breider, T. J., Atlas, E., Montzka, S. A., Miller, B. R., Moore, F., and Elkins, J.: The contribution of natural and anthropogenic very short-lived species to stratospheric bromine, Atmos. Chem. Phys., 12, 371–380, doi:10.5194/acp-12-371-2012, 2012b.

Hossaini, R., Mantle, H., Chipperfield, M. P., Montzka, S. A., Hamer, P., Ziska, F., Quack, B., Krüger, K., Tegtmeier, S., Atlas, E., Sala, S., Engel, A., Bönisch, H., Keber, T., Oram, D., Mills, G., Ordóñez, C., Saiz-Lopez, A., Warwick, N., Liang, Q., Feng, W., Moore, F., Miller, B. R., Marécal, V., Richards, N. A. D., Dorf,

M., and Pfeilsticker, K.: Evaluating global emission inventories of biogenic bromocarbons, Atmos. Chem. Phys., 13, 11 819–11 838, doi:10.5194/acp-13-11819-2013, 2013.

Hossaini, R., Chipperfield, M. P., Montzka, S. A., Rap, A., Dhomse, S., and Feng, W.: Efficiency of short-lived halogens at influencing climate through depletion of stratospheric ozone, Nat. Geosci., 8, 186–190, doi:10.1038/ngeo2363, 2015a.

Hossaini, R., Chipperfield, M. P., Saiz-Lopez, A., Harrison, J. J., von Glasow, R., Sommariva, R., Atlas, E., Navarro, M., Montzka, S. A., Feng, W., Dhomse, S., Harth, C., Mühle, J., Lunder, C., O'Doherty, S., Young, D., Reimann, S., Vollmer, M. K., Krummel, P. B., and Bernath, P. F.: Growth in stratospheric chlorine from short-lived chemicals not controlled by the Montreal Protocol, Geophys. Res. Lett., 42, 4573—4580, doi:10.1002/2015GL063783, 2015b.

Hoyle, C. R., Marecal, V., Russo, M. R., Allen, G., Arteta, J., Chemel, C., Chipperfield, M. P., D'Amato, F., Dessens, O., Feng, W., Hamilton, J. F., Harris, N. R. P., Hosking, J. S., Lewis, A. C., Morgenstern, O., Peter, T., Pyle, J. A., Reddmann, T., Richards, N. A. D., Telford, P. J., Tian, W., Viciani, S., Volz-Thomas, A., Wild, O., Yang, X., and Zeng, G.: Representation of tropical deep convection in atmospheric models - Part 2: Tracer transport, Atmos. Chem. Phys., 11, 8103–8131, doi:10.5194/acp-11-8103-2011, 2011.

Hughes, C., Johnson, M., von Glasow, R., Chance, R., Atkinson, H., Souster, T., Lee, G. A., Clarke, A., Meredith, M., Venables, H. J., Turner, S. M., Malin, G., and Liss, P. S.: Climate-induced change in biogenic bromine emissions from the Antarctic marine biosphere, Global Biogeochem. Cycles, 26, GB3019, doi:10.1029/2012GB004295, 2012.

Jöckel, P., Tost, H., Pozzer, A., Brühl, C., Buchholz, J., Ganzeveld, L., Hoor, P., Kerkweg, A., Lawrence, M. G., Sander, R., Steil, B., Stiller, G., Tanarhte, M., Taraborrelli, D., van Aardenne, J., and Lelieveld, J.: The atmospheric chemistry general circulation model ECHAM5/MESSy1: consistent simulation of ozone from the surface to the mesosphere, Atmos. Chem. Phys., 6, 5067–5104, doi:10.5194/acp-6-5067-2006, 2006.

Jöckel, P., Kerkweg, A., Pozzer, A., Sander, R., Tost, H., Riede, H., Baumgaertner, A., Gromov, S., and Kern, B.: Development cycle 2 of the Modular Earth Submodel System (MESSy2), Geosci. Model Dev., 3, 717–752, doi:10.5194/gmd-3-717-2010, 2010.

Krüger, K. and Quack, B.: Introduction to special issue: the TransBrom Sonne expedition in the tropical West Pacific, Atmos. Chem. Phys., 13, 9439–9446, doi:10.5194/acp-13-9439-2013, 2013.

Lacis, A. A., Wuebbles, D. J., and Logan, J. A.: Radiative forcing of climate by changes in the vertical distribution of ozone, J. Geophys. Res., 95, 9971-9981, doi:10.1029/JD095iD07p09971, 1990.

Laube, J. C., Engel, A., Boenisch, H., Moebius, T., Worton, D. R., Sturges, W. T., Grunow, K., and Schmidt, U.: Contribution of very short-lived organic substances to stratospheric chlorine and bromine in the tropics - a case study, Atmos. Chem. Phys., 8, 7325–7334, 2008.

Law, R. M., Rayner, P. J., Denning, A. S., Erickson, D., Fung, I. Y., Heimann, M., Piper, S. C., Ramonet, M., Taguchi, S., Taylor, J. A., Trudinger, C. M., and Watterson, I. G.: Variations in modelled atmospheric transport of carbon dioxide and the consequences for CO_2 inversions, Global Biogeochem. Cy., 10, 783–796, 1996.

Law, R. M., Peters, W., Rödenbeck, C., Aulagnier, C., Baker, I., Bergmann, D. J., Bousquet, P., Brandt, J., Bruhwiler, L., Cameron-Smith, P. J., Christensen, J. H., Delage, F., Denning, A. S., Fan, S., Geels, C., Houweling, S., Imasu, R., Karstens, U., Kawa, S. R., Kleist, J., Krol, M. C., Lin, S. J., Lokupitiya, R., Maki, T., Maksyu-

tov, S., Niwa, Y., Onishi, R., Parazoo, N., Patra, P. K., Pieterse, G., Rivier, L., Satoh, M., Serrar, S., Taguchi, S., Takigawa, M., Vautard, R., Vermeulen, A. T., and Zhu, Z.: TransCom model simulations of hourly atmospheric CO_2: Experimental overview and diurnal cycle results for 2002, Global Biogeochem. Cy., 22, GB3009, doi:10.1029/2007gb003050, 2008.

Leedham, E. C., Hughes, C., Keng, F. S. L., Phang, S.-M., Malin, G., and Sturges, W. T.: Emission of atmospherically significant halocarbons by naturally occurring and farmed tropical macroalgae, Biogeosciences, 10, 3615–3633, doi:10.5194/bg-10-3615-2013, 2013.

Lennartz, S. T., Krysztofiak, G., Marandino, C. A., Sinnhuber, B.-M., Tegtmeier, S., Ziska, F., Hossaini, R., Krüger, K., Montzka, S. A., Atlas, E., Oram, D. E., Keber, T., Bönnisch, H., and Quack, B.: Modelling marine emissions and atmospheric distributions of halocarbons and dimethyl sulfide: the influence of prescribed water concentration vs. prescribed emissions, Atmos. Chem. Phys., 15, 11753-11772, doi:10.5194/acp-15-11753-2015, 2015.

Levine, J. G., Braesicke, P., Harris, N. R. P., Savage, N. H., and Pyle, J. A.: Pathways and timescales for troposphere-to-stratosphere transport via the tropical tropopause layer and their relevance for very short lived substances, J. Geophys. Res., 112, doi:10.1029/2005JD006940, 2007.

Liang, Q., Atlas, E., Blake, D., Dorf, M., Pfeilsticker, K., and Schauffler, S.: Convective transport of very short lived bromocarbons to the stratosphere, Atmos. Chem. Phys., 14, 5781–5792, doi:10.5194/acp-14-5781-2014, 2014.

Liang, Q., Stolarski, R. S., Kawa, S. R., Nielsen, J. E., Douglass, A. R., Rodriguez, J. M., Blake, D. R., Atlas, E. L., and Ott, L. E.: Finding the missing stratospheric Br_y: a global modeling study of $CHBr_3$ and CH_2Br_2, Atmos. Chem. Phys., 10, 2269–2286, 2010.

Lock, A., Brown, A., Bush, M., Martin, G., and Smith, R.: A new boundary layer mixing scheme. Part I: Scheme description and single-column model tests, Mon. Weather Rev., 128, 3187–3199, 2000.

Mellor, G. L. and Yamada, A.: A hierarchy of turbulence closure models for planetary boundary layers, J. Atmos. Sci., 31, 1791– 1806, 1974.

Montzka, S. A., Krol, M., Dlugokencky, E., Hall, B., Jöckel, P., and Lelieveld, J.: Small Interannual Variability of Global Atmospheric Hydroxyl, Science, 331, 67–69, doi:10.1126/science.1197640, 2011.

Morgenstern, O., Braesicke, P., O'Connor, F. M., Bushell, A. C., Johnson, C. E., Osprey, S. M., and Pyle, J. A.: Evaluation of the new UKCA climate-composition model - Part 1: The stratosphere, Geosci. Model Dev., 2, 43–57, doi:10.5194/gmd-2-43-2009, 2009.

Nightingale, P. D., Malin, G., Law, C. S., Watson, A. J., Liss, P. S., Liddicoat, M. I., Boutin, J., and Upstill-Goddard, R. C.: In situ evaluation of air-sea gas exchange parameterizations using novel conservative and volatile tracers, Glob. Biogeochem. Cy., 14, 373—387, 2000.

Nordeng, T. E.: Extended versions of the convective parametrization scheme at ECMWF and their impact on the mean and transient activity of the model in the tropics. Technical Momorandum 206, ECMWF Research Department, European Centre for Medium Range Weather Forecasts, Reading, UK, 1994.

Orbe, C., Waugh, D. W., and Newman, P. A.: Air-mass origin in the tropical lower stratosphere: The influence of Asian boundary layer air, Geophys. Res. Lett., 42, 4240–4248, doi:10.1002/2015GL063937, 2015.

Ordóñez, C., Lamarque, J.-F., Tilmes, S., Kinnison, D. E., Atlas, E. L., Blake, D. R., Santos, G. S., Brasseur, G., and Saiz-Lopez, A.: Bromine and iodine chemistry in a global chemistry-climate model:

description and evaluation of very short-lived oceanic sources, Atmos. Chem. Phys., 12, 1423–1447, doi:10.5194/acp-12-1423-2012, 2012.

Orlikowska, A. and Schulz-Bull, D.: Seasonal variations of volatile organic compounds in the coastal Baltic Sea, Envir. Chem., 6, doi:10.1071/EN09107, 2009.

Patra, P. K., Law, R. M., Peters, W., Rodenbeck, C., Takigawa, M., Aulagnier, C., Baker, I., Bergmann, D. J., Bousquet, P., Brandt, J., Bruhwiler, L., Cameron-Smith, P. J., Christensen, J. H., Delage, F., Denning, A. S., Fan, S., Geels, C., Houweling, S., Imasu, R., Karstens, U., Kawa, S. R., Kleist, J., Krol, M. C., Lin, S.-J., Lokupitiya, R., Maki, T., Maksyutov, S., Niwa, Y., Onishi, R., Parazoo, N., Pieterse, G., Rivier, L., Satoh, M., Serrar, S., Taguchi, S., Vautard, R., Vermeulen, A. T., and Zhu, Z.: TransCom model simulations of hourly atmospheric CO_2: analysis of synoptic-scale variations for the period 2002–2003, Global Biogeochem. Cy., 22, GB4013, doi:10.1029/2007GB003081, 2008.

Patra, P. K., Takigawa, M., Dutton, G. S., Uhse, K., Ishijima, K., Lintner, B. R., Miyazaki, K., and Elkins, J. W.: Transport mechanisms for synoptic, seasonal and interannual SF_6 variations and "age" of air in troposphere, Atmos. Chem. Phys., 9, 1209–1225, doi:10.5194/acp-9-1209-2009, 2009.

Patra, P. K., Houweling, S., Krol, M., Bousquet, P., Belikov, D., Bergmann, D., Bian, H., Cameron-Smith, P., Chipperfield, M. P., Corbin, K., Fortems-Cheiney, A., Fraser, A., Gloor, E., Hess, P., Ito, A., Kawa, S. R., Law, R. M., Loh, Z., Maksyutov, S., Meng, L., Palmer, P. I., Prinn, R. G., Rigby, M., Saito, R., and Wilson, C.: TransCom model simulations of CH_4 and related species: linking transport, surface flux and chemical loss with CH_4 variability in the troposphere and lower stratosphere, Atmos. Chem. Phys., 11, 12813–12837, doi:10.5194/acp-11-12813-2011, 2011.

Phang, S-M., Keng, FS-L., Paramjeet-Kaur, M. S., Lim, Y-K., Rahman, N. A., Leedham, E. C., Robinson, A. D., Harris, N. R. P., Pyle, J. A., and Sturges, W. T.: Can seaweed farming in the tropics contribute to climate change through emissions of short-lived halocarbons, Malaysian Journal of Science, 34, 8–19, 2015.

Pfeilsticker, K., Sturges, W. T., Bösch, H., Camy-Peyret, C., Chipperfield, M. P., Engel, A., Fitzenberger, R., Müller, M., Payan, S., and Sinnhuber, B.-M.: Lower stratospheric organic and inorganic bromine budget for the Artic winter 1998/99, Geophys. Res. Lett., 27, 20, 3305-3308, 2000.

Pisso, I., Haynes, P. H., and Law, K. S.: Emission location dependent ozone depletion potentials for very short-lived halogenated species, Atmos. Chem. Phys., 10, 12025–12036, doi:10.5194/acp-10-12025-2010, 2010.

Pyle, J. A., Ashfold, M. J., Harris, N. R. P., Robinson, A. D., Warwick, N. J., Carver, G. D., Gostlow, B., O'Brien, L. M., Manning, A. J., Phang, S. M., Yong, S. E., Leong, K. P., Ung, E. H., and Ong, S.: Bromoform in the tropical boundary layer of the Maritime Continent during OP3, Atmos. Chem. Phys., 11, 529–542, doi:10.5194/acp-11-529-2011, 2011.

Quack, B. and Wallace, D.: Air-sea flux of bromoform: Controls, rates, and implications, Global Biogeochem. Cycles, 17, doi:10.1029/2002GB001890, 2003.

Randel, W. J., Park, M., Emmons, L., Kinnison, D., Bernath, P., Walker, K. A., Boone, C., and Pumphrey, H.: Asian Monsoon Transport of Pollution to the Stratosphere, Science, 328, 611–613, doi:10.1126/science.1182274, 2010.

Riese, M., Ploeger, F., Rap, A., Vogel, B., Konopka, P., Dameris, M., and Forster, P.: Impact of uncertainties in atmospheric mixing on simulated UTLS composition and related radiative effects, J. Geophys. Res., 117, D16305, doi:10.1029/2012JD017751, 2012.

Robinson, A. D., Harris, N. R. P., Ashfold, M. J., Gostlow, B., Warwick, N. J., O'Brien, L. M., Beardmore, E. J., Nadzir, M. S. M., Phang, S. M., Samah, A. A., Ong, S., Ung, H. E., Peng, L. K., Yong, S. E., Mohamad, M., and Pyle, J. A.: Long-term halocarbon observations from a coastal and an inland site in Sabah, Malaysian Borneo, Atmos. Chem. Phys., 14, 8369–8388, doi:10.5194/acp-14-8369-2014, 2014.

Roeckner, E., Brokopf, R., Esch, M., Giorgetta, M., Hagemann, S., Kornblueh, L., Manzini, E., Schlese, U., and Schulzweida, U.: Sensitivity of simulated climate to horizontal and vertical resolution in the ECHAM5 atmosphere model, J. Climate, 19, 3771–3791, doi:10.1175/JCLI3824.1, 2006.

Russo, M. R., Ashfold, M. J., Harris, N. R. P., and Pyle, J. A.: On the emissions and transport of bromoform: sensitivity to model resolution and emission location, Atmos. Chem. Phys., 15, 14031–14040, doi:10.5194/acp-15-14031-2015, 2015.

Rybka, H. and Tost, H.: Uncertainties in future climate predictions due to convection parameterisations, Atmos. Chem. Phys., 14, 5561–5576, doi:10.5194/acp-14-5561-2014, 2014.

Sala, S., Bönisch, H., Keber, T., Oram, D. E., Mills, G., and Engel, A.: Deriving an atmospheric budget of total organic bromine using airborne in situ measurements from the western Pacific area during SHIVA, Atmospheric Chemistry and Physics, 14, 6903–6923, doi:10.5194/acp-14-6903-2014, 2014.

Salawitch, R., Weisenstein, D., Kovalenko, L., Sioris, C., Wennberg, P., Chance, K., Ko, M., and McLinden, C.: Sensitivity of ozone to bromine in the lower stratosphere, Geophys. Res. Lett., 32, L05811, doi:10.1029/2004GL021504, 2005.

Sander, S., Friedl, R., Barker, J., Golden, D., Kurylo, M., Wine, P., Abbatt, J., Burkholder, J., Kolb, C., Moortgat, G., Huie, R., and Orkin, V.: Chemical Kinetics and Photochemical Data for Use in Atmospheric Studies, Evaluation Number 17, JPL Publication 10-6, Jet Propulsion Laboratory, 2011.

Sinnhuber, B.-M. and Meul, S.: Simulating the impact of emissions of brominated very short lived substances on past stratospheric ozone trends, Geophys. Res. Lett., 42, 2449–2456, doi:10.1002/2014GL062975, 2015.

Sinnhuber, B.-M., Sheode, N., Sinnhuber, M., Chipperfield, M. P., and Feng, W.: The contribution of anthropogenic bromine emissions to past stratospheric ozone trends: a modelling study, Atmos. Chem. Phys., 9, 2863–2871, 2009.

Stemmler, I., Hense, I., and Quack, B.: Marine sources of bromoform in the global open ocean – global patterns and emissions, Biogeosciences, 12, 1967–1981, doi:10.5194/bg-12-1967-2015, 2015.

Sturges, W., Oram, D., Carpenter, L., Penkett, S., and Engel, A.: Bromoform as a source of stratospheric bromine, Geophys. Res. Lett., 27, 2081–2084, doi:10.1029/2000GL011444, 2000.

Taguchi, S.: A three-dimensional model of atmospheric CO2 transport based on analyzed winds: Model description and simulation results for TRANSCOM, J. Geophys Res., 101, 15099–15109, doi:10.1029/96JD00504, 1996.

Taguchi, S., Tasaka, S., Matsubara, M., Osada, K., Yokoi, T., and Yamanouchi, T.: Air-sea gas transfer rate for the Southern Ocean inferred from 222Rn concentrations in maritime air and a global atmospheric transport model, J. Geophys. Res., 118, 7606–7616, doi:10.1002/jgrd.50594, 2013.

Tegtmeier, S., Krüger, K., Quack, B., Atlas, E. L., Pisso, I., Stohl, A., and Yang, X.: Emission and transport of bromocarbons: from the West Pacific ocean into the stratosphere, Atmos. Chem. Phys, 12, 10 633–10 648, doi:10.5194/acp-12-10633-2012, 2012.

Tegtmeier, S., Krüger, K., Quack, B., Atlas, E., Blake, D. R., Boenisch, H., Engel, A., Hepach, H., Hossaini, R., Navarro, M. A., Raimund, S., Sala, S., Shi, Q., and Ziska, F.: The contribution of oceanic methyl iodide to stratospheric iodine, Atmos. Chem. Phys., 13, 11869–11886, doi:10.5194/acp-13-11869-2013, 2013.

Tegtmeier, S., Ziska, F., Pisso, I., Quack, B., Velders, G. J. M., Yang, X., and Krüger, K.: Oceanic bromine emissions weighted by their ozone depletion potential, Atmos. Chem. Phys., 15, 13647–13663, doi:10.5194/acp-15-13647-201, 2015.

Tiedtke, M.: A comprehensive mass flux scheme for cumulus parameterization in large-scale models, Mon. Weather Rev., 117, 1779–1800, doi:10.1175/1520-0493, 1989.

Tilmes, S., Kinnison, D. E., Garcia, R. R., Salawitch, R., Canty, T., Lee-Taylor, J., Madronich, S., and Chance, K.: Impact of very short-lived halogens on stratospheric ozone abundance and UV radiation in a geo-engineered atmosphere, Atmos. Chem. Phys., 12, 10 945–10 955, doi:10.5194/acp-12-10945-2012, 2012.

Tissier, A.-S. and Legras, B.: Transport across the tropical tropopause layer and convection, Atmos. Chem. Phys., 16, 3383–3398, doi:10.5194/acp-16-3383-2016, 2016.

Thompson, R. L., Patra, P. K., Ishijima, K., Saikawa, E., Corazza, M., Karstens, U., Wilson, C., Bergamaschi, P., Dlugokencky, E., Sweeney, C., Prinn, R. G., Weiss, R. F., O'Doherty, S., Fraser, P. J., Steele, L. P., Krummel, P. B., Saunois, M., Chipperfield, M., and Bousquet, P.: TransCom N_2O model inter-comparison – Part 1: Assessing the influence of transport and surface fluxes on tropospheric N_2O variability, Atmos. Chem. Phys., 14, 4349-4368, doi:10.5194/acp-14-4349-2014, 2014.

Vogel, B., Günther, G., Müller, R., Grooß, J.-U., Hoor, P., Krämer, M., Müller, S., Zahn, A., and Riese, M.: Fast transport from Southeast Asia boundary layer sources to northern Europe: rapid uplift in typhoons and eastward eddy shedding of the Asian monsoon anticyclone, Atmos. Chem. Phys., 14, 12745—12762, doi:10.5194/acp-14-12745-2014, 2014.

Warwick, N. J., Pyle, J. A., Carver, G. D., Yang, X., Savage, N. H., O'Connor, F. M., and Cox, R. A.: Global modeling of biogenic bromocarbons, J. Geophys. Res., 111, doi:10.1029/2006JD007264, 2006.

Werner, B., Atlas, E., Cheung, R., Chipperfield, M. P., Colosimo, F., Daube, B., Deutschmann, T., Elkins, J. W., Fahey, D. W., Feng, W., Festa, J., Gao, R-S., Hintsa, E. J., Hossaini, R., Moore, F. L., Navarro, M. A., Pittman, J., Raecke, R., Scalone, L., Spolaor, M., Stutz, J., Thornberry, T. D., Tsai, C., Wofsy, S., and Pfeilsticker, K.: Probing the subtropical lowermost stratosphere, tropical upper troposphere, and tropopause layer for inorganic bromine, paper in preparation for Atmos. Chem. Phys. Discuss.

Wisher, A., Oram, D. E., Laube, J. C., Mills, G. P., van Velthoven, P., Zahn, A., and Brenninkmeijer, C. A. M.: Very short-lived bromomethanes measured by the CARIBIC observatory over the North Atlantic, Africa and Southeast Asia during 2009–2013, Atmos. Chem. Phys., 14, 3557–3570, doi:10.5194/acp-14-3557-2014, 2014.

WMO: Scientific Assessment of Ozone Depletion: 2014, Global Ozone Research and Monitoring Project, Report No. 55, World Meteorological Organization, Geneva, Switzerland. , 2014.

Wofsy, S. C., Team, H. S., Team, C. M., and Team, S.: HIAPER Pole-to-Pole Observations (HIPPO): fine-grained, global-scale measurements of climatically important atmospheric gases and aerosols, Phil. Trans., 369, 2073–2086, doi:10.1098/rsta.2010.0313, 2011.

Wolter, K. and Timlin, M. S.: Measuring the strength of ENSO events: How does 1997/98 rank?, Weather, 53, 315–324, doi:10.1002/j.1477-8696.1998.tb06408.x, 1998.

Yang, X., Abraham, N. L., Archibald, A. T., Braesicke, P., Keeble, J., Telford, P. J., Warwick, N. J., and Pyle, J. A.: How sensitive is the recovery of stratospheric ozone to changes in concentrations of very short-lived bromocarbons?, Atmos. Chem. Phys., 14, 10 431–10 438, doi:10.5194/acp-14-10431-2014, 2014.

Zhang, K., Wan, H., Zhang, M., and Wang, B.: Evaluation of the atmospheric transport in a GCM using radon measurements: sensitivity to cumulus convection parameterization, Atmos. Chem. Phys., 8, 2811–2832, doi:10.5194/acp-8-2811-2008, 2008.

Zhang, G. J. and McFarlane, N. A.: Sensitivity of climate simulations to the parameterization of cumulus convection in the Canadian climate centre general circulation model, Atmos. Ocean, 33, 407–446, 1995.

Ziska, F., Quack, B., Abrahamsson, K., Archer, S. D., Atlas, E., Bell, T., Butler, J. H., Carpenter, L. J., Jones, C. E., Harris, N. R. P., Hepach, H., Heumann, K. G., Hughes, C., Kuss, J., Krüger, K., Liss, P., Moore, R. M., Orlikowska, A., Raimund, S., Reeves, C. E., Reifenhäuser, W., Robinson, A. D., Schall, C., Tanhua, T., Tegtmeier, S., Turner, S., Wang, L., Wallace, D., Williams, J., Yamamoto, H., Yvon-Lewis, S., and Yokouchi, Y.: Global sea-to-air flux climatology for bromoform, dibromomethane and methyl iodide, Atmos. Chem. Phys., 13, 8915–8934, doi:10.5194/acp-13-8915-2013, 2013.

Table 1 Summary of the VSLS tracers simulated by the models, the global total emission flux (Gg VSLS yr^{-1}) and the rate constant for their reaction with OH (Sander et al., 2011). See text for details of emission inventories.

Tracer #	Species	Tracer name	Ocean emission inventory		Rate constant (VSLS + OH reaction)
			Global flux (Gg yr^{-1})	Reference	k(T) (cm^3 molec^{-1} s^{-1})
1	Bromoform	CHBr$_3$_L	450	Liang et al. (2010)	1.35×10^{-12}exp(-600/T)
2		CHBr$_3$_O	530	Ordóñez et al. (2012)	
3		CHBr$_3$_Z	216	Ziska et al. (2013)	
4	Dibromomethane	CH$_2$Br$_2$_L	62	Liang et al. (2010)	2.00×10^{-12}exp(-840/T)
5		CH$_2$Br$_2$_O	67	Ordóñez et al. (2012)	
6		CH$_2$Br$_2$_Z	87	Ziska et al. (2013)	

Table 2 Overview of TransCom-VSLS models and model variants.

#	Model[1]	Institution[2]	Resolution		Meteorology[5]	BL mix.	Convection	Reference
			Horizontal[3]	Vertical[4]				
1	ACTM	JAMSTEC	2.8°×2.8°	67σ	JRA-25	Mellor and Yamada (1974)	Arakawa and Shubert (1974)	Patra et al. (2009)
2	B3DCTM	UoB	3.75°×2.5°	40 σ-θ	ECMWF ERA-Interim	Simple[7]	ERA-Interim, archived[8]	Aschmann et al. (2014)
3	**EMAC**[6](_free)	KIT	2.8°×2.8°	39 σ-p	Online, free-running	Jöckel et al. (2006)	Tiedtke (1989) [9]	Jöckel et al. (2006, 2010)
4	*EMAC* (_nudged)	KIT	2.8°×2.8°	39 σ-p	Nudged to ERA-Interim	Jöckel et al. (2006)	Tiedtke (1989) [9]	Jöckel et al. (2006, 2010)
5	MOZART	EMU	2.5°×1.9°	56 σ-p	MERRA	Holtslag and Boville (1993)	Note 10	Emmons et al. (2010)
6	NIES-TM	NIES	2.5°×2.5°	32 σ-θ	JCDAS (JRA-25)	Belikov et al. (2013)	Tiedtke (1989)	Belikov et al. (2011, 2013)
7	STAG	AIST	1.125°×1.125°	60 σ-p	ECMWF ERA-Interim	Taguchi et al. (2013)	Taguchi et al. (2013)	Taguchi (1996)
8	TOMCAT	UoL	2.8°×2.8°	60 σ-p	ECMWF ERA-Interim	Holtslag and Boville (1993)	Tiedtke (1989)	Chipperfield (2009)
9	*TOMCAT* (_conv)	UoL	2.8°×2.8°	60 σ-p	ECMWF ERA-Interim	Holtslag and Boville (1993)	ERA-Interim, archived[8]	Chipperfield (2009)
10	**UKCA** (_low)	UoC/NCAS	3.75°×2.5°	60 σ-z	Online, free-running	Lock et al. (2000)	Gregory and Rowntree (1990)	Morgenstern et al. (2009)
11	*UKCA* (_high)	UoC/NCAS	1.875°×1.25°	85 σ-z	Online, free-running	Lock et al. (2000)	Gregory and Rowntree (1990)	Morgenstern et al. (2009)

[1] All models are offline CTMs except bold entries which are CCMs. Model variants are shown in italics.
CCMs ran using prescribed sea surface temperatures from observations.

[2] JAMSTEC: Japan Agency for Marine-Earth Science and Technology, Japan; UoB: University of Bremen, Germany; KIT: Karlsruhe Institute of Technology,
Germany; EMU: Emory University, USA ; NIES: National Institute for Environmental Studies, Japan; AIST: National Institute of Advanced
Industrial Science and Technology, Japan; UoL: University of Leeds, UK; UoC: University of Cambridge, UK; NCAS: National Centre for
Atmospheric Science, UK.

[3] Longitude×latitude

[4] σ: terrain-following sigma levels (pressure divided by surface pressure); σ-p: hybrid sigma-pressure; σ-θ: hybrid sigma-potential
temperature; σ-z: hybrid sigma-height.

[5] MERRA: Modern-era Retrospective Analysis for Research and Applications; JCDAS: Japan Meteorological Agency Climate Data
Assimilation System; JRA-25: Japanese 25-year ReAnalysis; ECMWF: European Center for Medium range Weather Forecasting.

[6] ECHAM/MESSy Atmospheric Chemistry (EMAC) model (Roeckner et al., 2006). ECHAM5 version 5.3.02. MESSy version 2.42.

[7] Simple averaging of tracer mixing ratio below ERA-Interim boundary layer height.

[8] Read-in convective massfluxes from ECMWF ERA-Interim. See Aschmann et al. (2011) for B3DCTM implementation and Feng et al. (2011) for TOMCAT implementation.

[9] With modifications from Nordeng (1994).

[10] Shallow & mid-level convection (Hack , 1994); deep convection (Zhang and McFarlane, 1995).

Table 3 Summary and location of ground-based surface VSLS measurements used in TransCom-VSLS, arranged from north to south. All sites are part of the NOAA/ESRL global monitoring network, with the exception of TAW, at which measurements were obtained by the University of Cambridge (see main text). *Stations SUM, MLO and SPO elevated at ∼3210m, 3397m and 2810m, respectively.

Station	Site Name	Latitude	Longitude
ALT	Alert, NW Territories, Canada	82.5° N	62.3° W
SUM*	Summit, Greenland	72.6° N	38.4° W
BRW	Pt. Barrow, Alaska, USA	71.3° N	156.6° W
MHD	Mace Head, Ireland	53.0° N	10.0° W
LEF	Wisconsin, USA	45.6° N	90.2° W
HFM	Harvard Forest, USA	42.5°N	72.2° W
THD	Trinidad Head, USA	41.0° N	124.0° W
NWR	Niwot Ridge, Colorado, USA	40.1° N	105.6° W
KUM	Cape Kumukahi, Hawaii, USA	19.5° N	154.8° W
MLO*	Mauna Loa, Hawaii, USA	19.5° N	155.6° W
TAW	Tawau, Sabah, Malaysian Borneo	4.2° N	117.9° E
SMO	Cape Matatula, American Samoa	14.3° S	170.6° W
CGO	Cape Grim, Tasmania, Australia	40.7° S	144.8° E
PSA	Palmer Station, Antarctica	64.6° S	64.0° W
SPO*	South Pole	90.0° S	-

Table 4 Correlation coefficient (r) between the observed and simulated climatological monthly mean surface CHBr$_3$ volume mixing ratio (at ground-based monitoring sites, Table 3). Model output based on CHBr$_3$_L tracer (i.e. using aseasonal emissions inventory of Liang et al. (2010)). Stations in bold denote where virtually all models fail to reproduce phase of the observed CHBr$_3$ seasonal cycle.

Site	ACTM	B3DCTM	EMAC_F	EMAC_N	MOZART	NIES	STAG	TOMCAT	UKC_LO	UKCA_HI
ALT	0.91	0.90	0.89	0.89	0.95	0.93	0.60	0.94	0.92	0.94
SUM	0.69	0.73	0.71	0.70	0.84	0.71	0.40	0.73	0.75	0.88
BRW	0.96	0.97	0.89	0.91	0.99	0.98	0.73	0.97	0.94	0.97
MHD	−0.89	−0.89	−0.93	−0.89	−0.85	−0.89	−0.79	−0.90	−0.91	−0.73
LEF	0.84	0.72	0.74	0.78	0.83	0.74	0.35	0.43	0.78	0.88
HFM	0.64	0.61	0.66	0.69	0.79	0.46	0.08	0.58	0.40	0.81
THD	−0.87	−0.65	−0.58	−0.42	0.26	−0.65	−0.63	−0.51	−0.48	−0.12
NWR	0.92	0.91	0.91	0.93	0.98	0.94	0.74	0.94	0.92	0.93
KUM	0.74	0.74	0.72	0.73	0.78	0.70	0.57	0.74	0.74	0.69
MLO	0.94	0.97	0.99	0.98	0.98	0.95	0.95	0.99	0.95	0.93
TAW	−0.27	−0.08	0.17	−0.05	−0.34	−0.07	−0.15	0.23	0.13	0.22
SMO	0.56	0.45	0.43	0.72	0.32	0.23	0.04	0.72	0.59	−0.19
CGO	−0.64	0.72	−0.22	−0.18	−0.53	0.31	0.85	−0.71	−0.72	−0.35
PSA	0.13	0.24	0.60	0.44	0.40	-0.39	0.16	0.14	0.09	0.62
SPO	0.90	0.91	0.85	0.89	0.94	0.41	0.71	0.92	0.93	0.88

Table 5 As Table 4 but for CH_2Br_2.

Site	ACTM	B3DCTM	EMAC_F	EMAC_N	MOZART	NIES	STAG	TOMCAT	UKCA_LO	UKCA_HI
ALT	0.90	0.97	0.79	0.82	0.96	0.98	0.77	0.94	0.85	0.96
SUM	0.71	0.93	0.75	0.76	0.92	0.91	0.87	0.77	0.79	0.96
BRW	0.87	0.92	0.82	0.85	0.93	0.91	0.90	0.88	0.93	0.93
MHD	−0.65	−0.73	−0.72	−0.69	−0.76	−0.75	−0.64	−0.72	−0.71	−0.76
LEF	0.87	0.73	0.84	0.84	0.94	0.94	0.47	0.62	0.88	0.96
HFM	0.82	0.79	0.83	0.84	0.95	0.90	−0.02	0.75	0.72	0.92
THD	0.54	0.80	0.73	0.79	0.78	0.84	0.04	0.69	0.66	0.75
NWR	0.90	0.88	0.91	0.89	0.99	0.97	0.86	0.91	0.92	0.97
KUM	0.90	0.89	0.90	0.91	0.99	0.91	0.74	0.90	0.92	0.98
MLO	0.90	0.89	0.94	0.91	0.96	0.90	0.30	0.91	0.93	0.97
TAW	−0.83	−0.80	−0.78	−0.75	−0.39	−0.47	−0.12	0.15	0.20	−0.16
SMO	−0.08	0.67	−0.14	0.59	0.38	−0.12	0.34	0.97	0.74	0.00
CGO	0.59	−0.43	0.45	0.30	0.64	−0.06	−0.42	0.80	0.80	0.41
PSA	0.17	0.71	0.52	0.68	0.75	0.08	0.62	0.72	0.65	0.68
SPO	0.88	0.91	0.82	0.86	0.95	−0.04	0.97	0.90	0.94	0.88
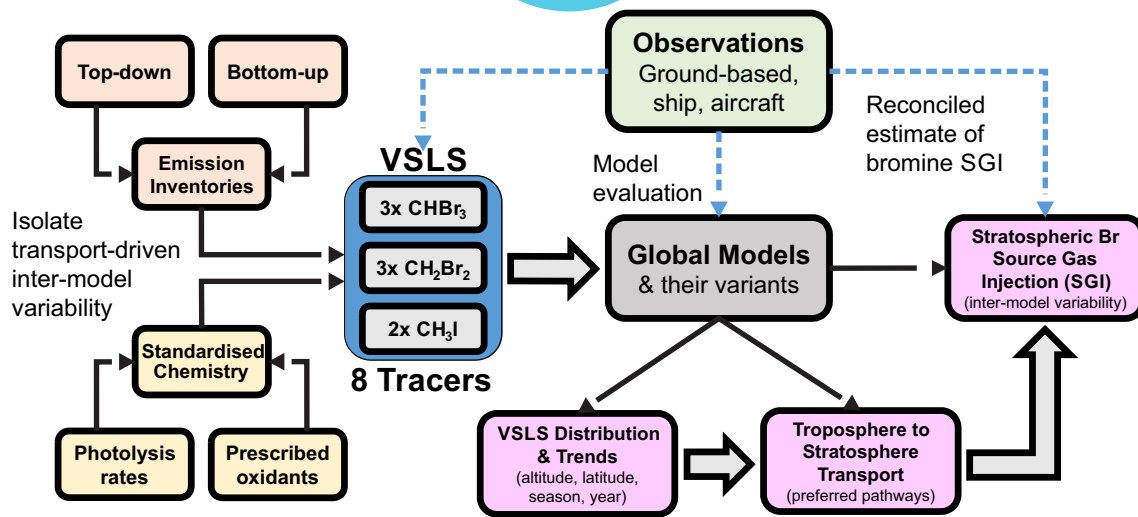
Figure 1. Schematic of the the TransCom-VSLS project approach.
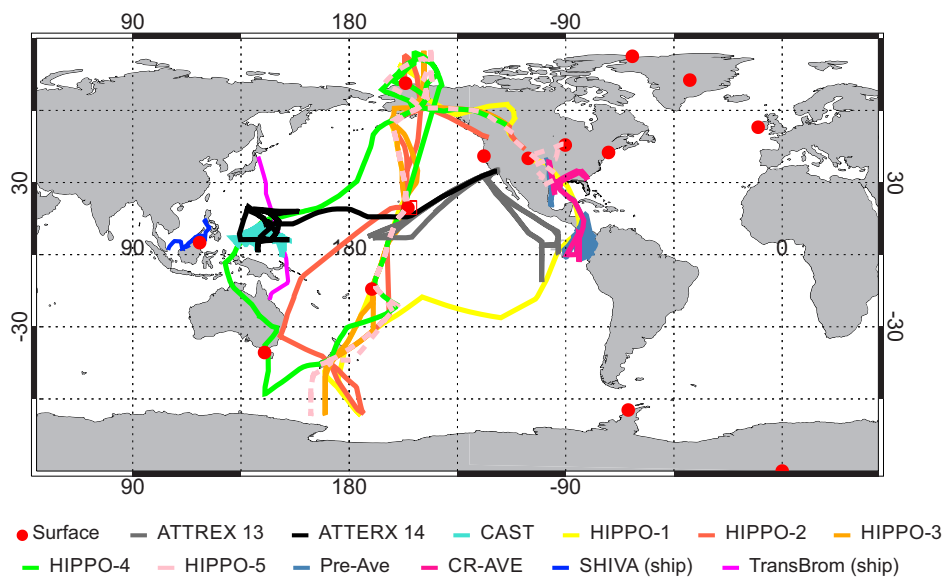
Figure 2. Summary of ground-based and campaign data used in TransCom-VSLS. See main text for details.
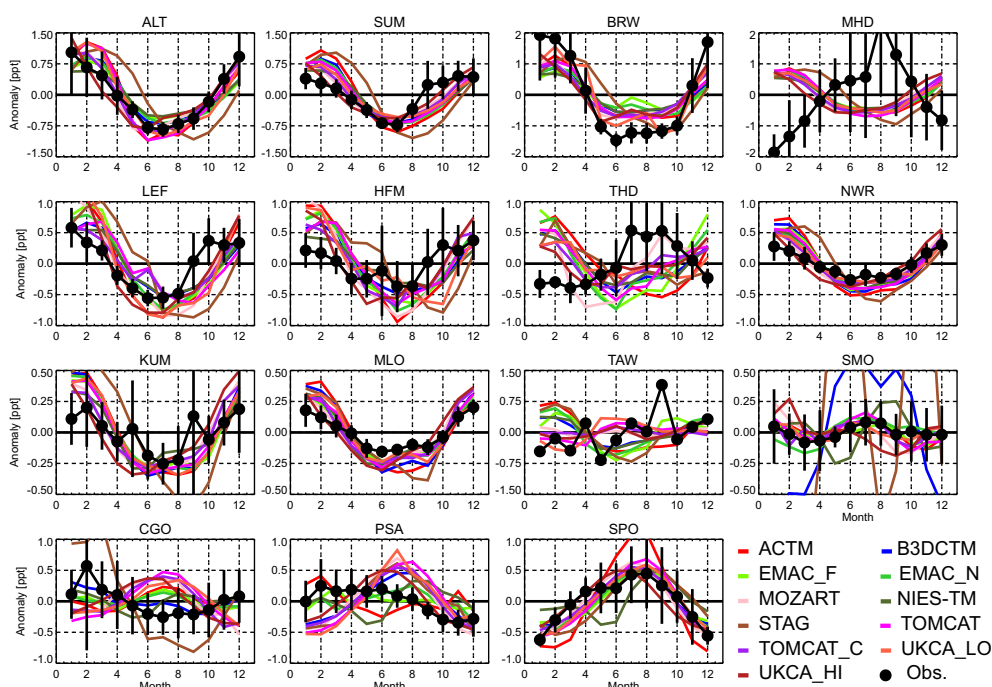
Figure 3. Comparison of the observed and simulated seasonal cycle of surface CHBr₃ at ground-based measurement sites (see Table 3). The seasonal cycle is shown here as climatological (1998-2011) monthly mean anomalies, calculated by subtracting the climatological monthly mean CHBr₃ mole fraction (ppt) from the climatological annual mean, in both the observed (black points) and model (coloured lines, see legend) data sets. The location of the surface sites is summarised in Table 3. Model output based on CHBr₃_L tracer (i.e. using aseasonal emissions inventory of Liang et al. (2010)). Horizontal bars denote ±1σ.
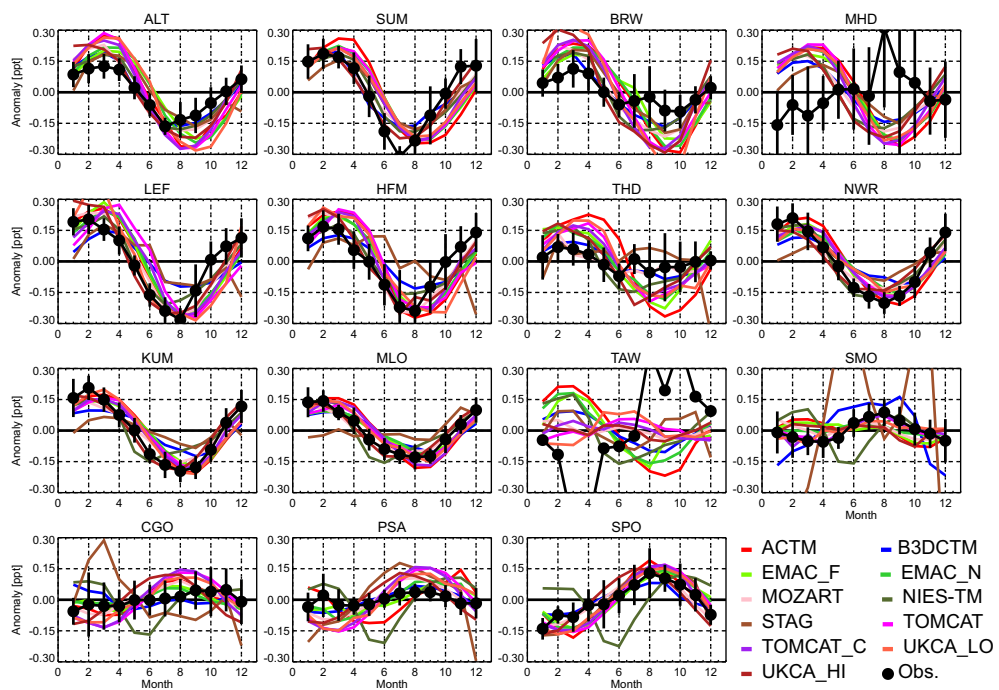
Figure 4. As Figure 3 but for CH_2Br_2.
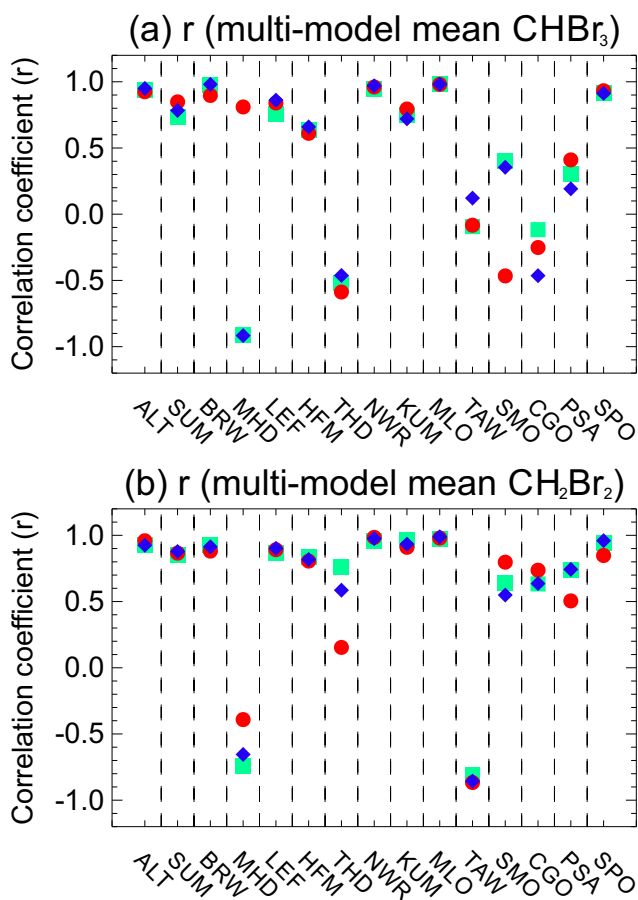
Figure 5. Correlation coefficient (r) between observed and multi-model mean (a) $CHBr_3$ and (b) CH_2Br_2, at ground-based monitoring sites. The correlation here represents the mean annual seasonal variation. At each site, $3 \times r$ values are given, reflecting the 3 different model $CHBr_3$ tracers; green squares denote the $CHBr_3$_L tracer (top-down derived Liang et al. (2010) emissions), blue diamonds denote the $CHBr_3$_O tracer (top-down Ordóñez et al. (2012) emissions) and red circles denote the $CHBr_3$_Z tracer (bottom-up Ziska et al. (2013) emissions).
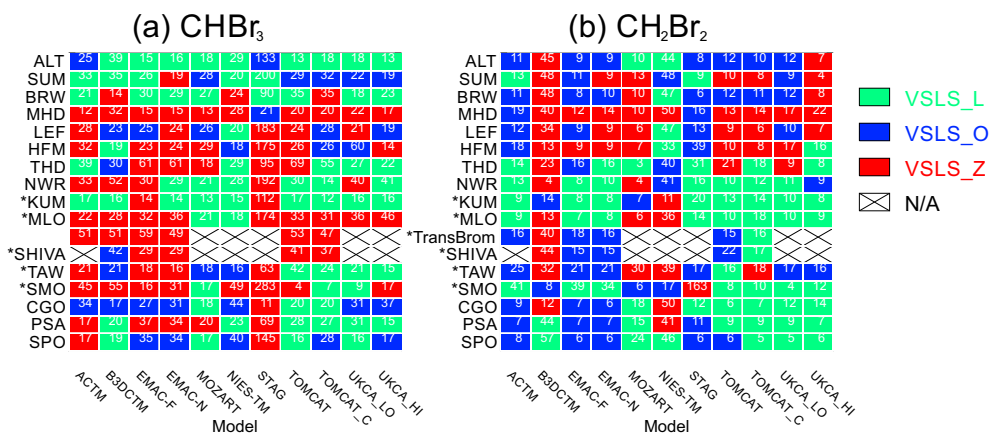
Figure 6. Summary of agreement between model (a) CHBr$_3$ and (b) CH$_2$Br$_2$ tracers and corresponding surface observations (ground-based, see Table 3, and TransBrom/SHIVA ship cruises). The fill colour of each cell (see legend) indicates the tracer giving the best agreement for that model, i.e. the lowest mean absolute percentage error (MAPE, see main text for details), and the numbers within the cells give the MAPE value (%), for each model compared to the observations. CHBr$_3$_L tracer used the Liang et al. (2010) emissions inventory, CHBr$_3$_O tracer used Ordóñez et al. (2012) and CHBr$_3$_Z tracer used Ziska et al. (2013). Sites marked with * are tropical locations. Certain model-measurement comparisons are not available (N/A).
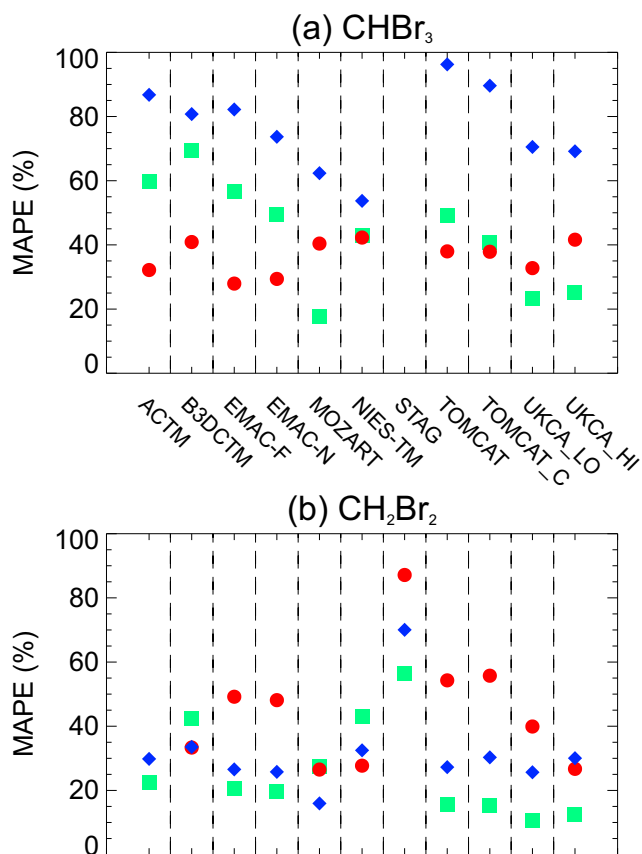
Figure 7. Overall mean absolute percentage error (MAPE) between model (a) CHBr$_3$ and (b) CH$_2$Br$_2$ tracers and corresponding surface observations, within the tropics only (i.e. sites KUM, MLO, TAW, SMO and the TransBrom and SHIVA ship cruises). Note, the scale is capped at 100%. A small number of data points fall outside of this range. Green squares denote the CHBr$_3$_L tracer, blue diamonds denote the CHBr$_3$_O tracer and red circles denote the CHBr$_3$_Z tracer.
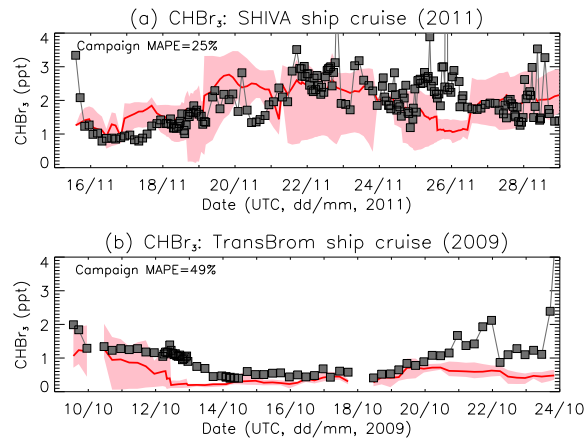
Figure 8. Comparison of modelled versus observed CHBr$_3$ surface volume mixing ratio (ppt) during (a) SHIVA (2011) and (b) TransBrom (2009) ship cruises. The multi-model mean is shown and the shaded region is the model spread. The mean absolute percentage error (MAPE) over each campaign is annotated.
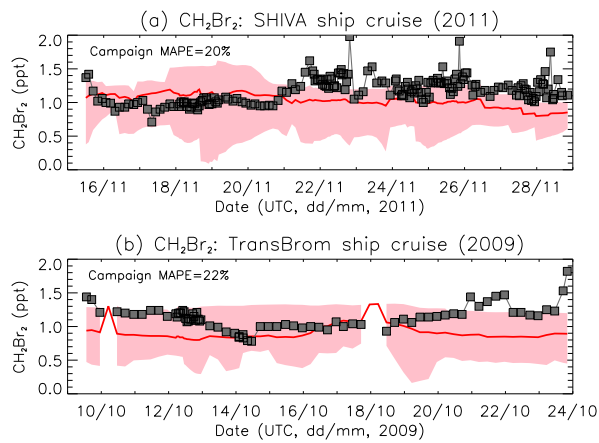
Figure 9. As Figure 8 but for CH$_2$Br$_2$.
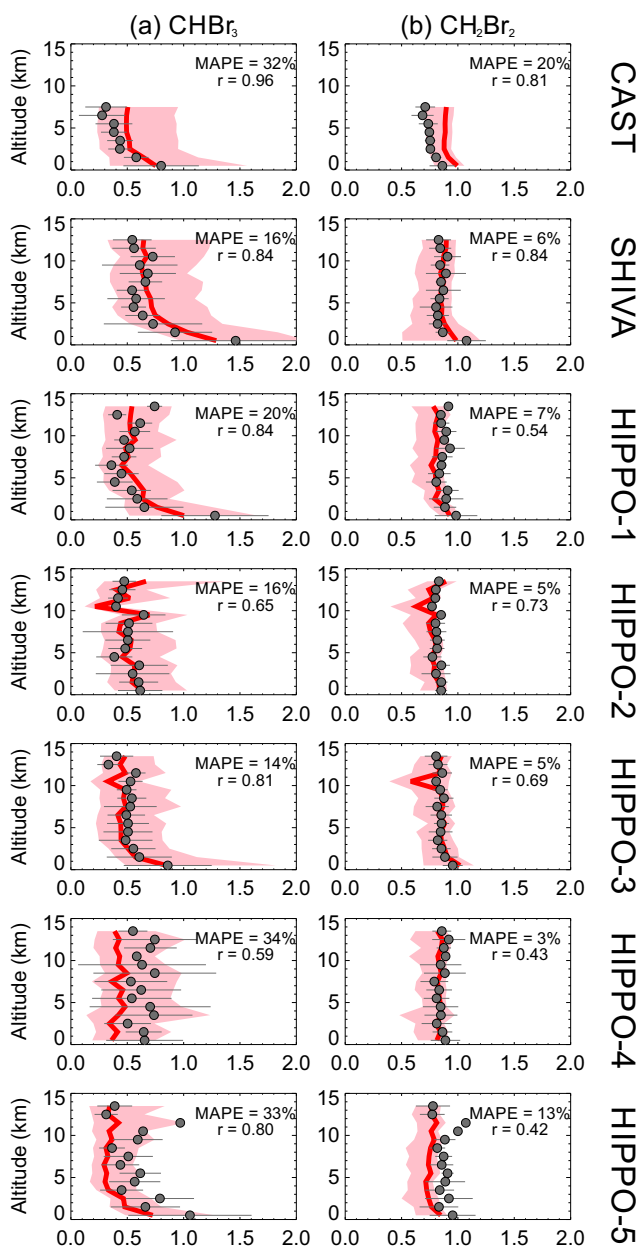
Figure 10. Compilation of modelled versus observed tropical profiles of (a) CHBr$_3$ and (b) CH$_2$Br$_2$ mixing ratio (ppt) from recent aircraft campaigns. Details of campaigns given in Section 2.4. Campaign mean observed profiles derived from tropical measurements only and averaged in 1 km vertical bins (filled circles). The horizontal bars denote $\pm 1\sigma$ from the observed mean. Shown is the corresponding multi-model mean profile (red) and model spread (shading). All models were included in the MMM with the exception of STAG (see Section 3.1.2). Models were sampled in the same space/time as the observed values, though for the comparison to CAST data, a climatological model profile is shown. The model-measurement correlation coefficient (r) and the mean absolute percentage error (MAPE, see main text) between the two are indicated in each panel.
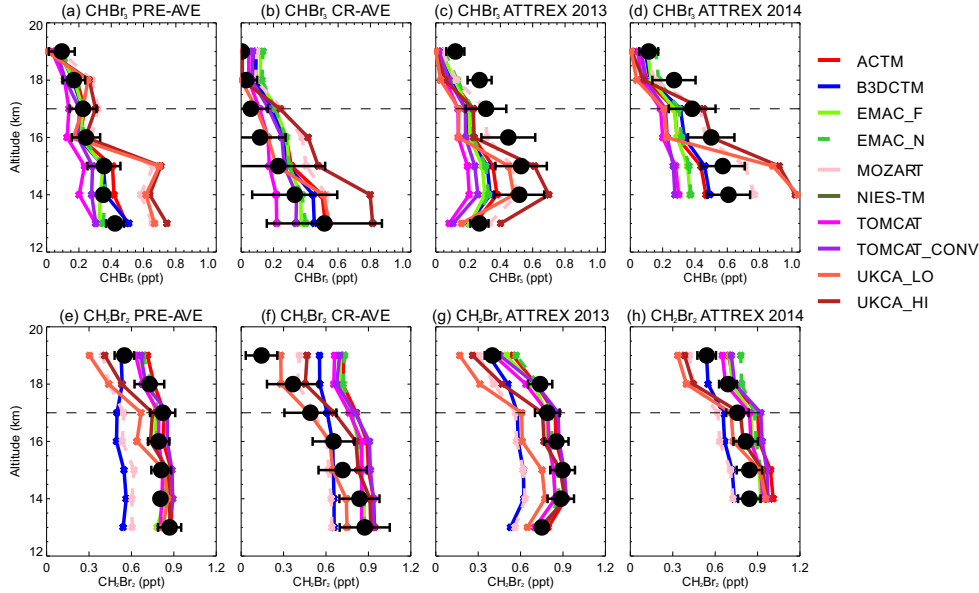
Figure 11. Comparison of modelled versus observed volume mixing ratio (ppt) of CHBr₃ (panels a-d) and CH₂Br₂ (panels e-h) from aircraft campaigns in the tropics (see main text for campaign details). The observed values (filled circles) are averages in 1 km altitude bins and the error bars denote $\pm 1\sigma$. The dashed line denotes the approximate cold point tropopause for reference.
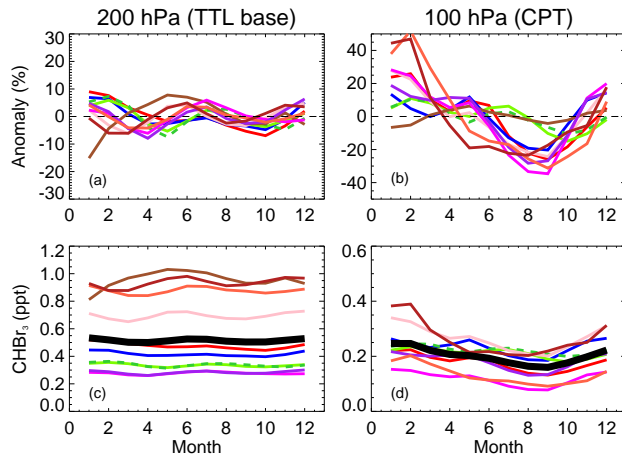
Figure 12. Simulated monthly mean anomalies of CHBr₃ volume mixing ratio (vmr), expressed as a percentage with respect to the annual mean, for (a) 200 hPa, the approximate base of the tropical tropopause layer (TTL) and (b) 100 hPa, the cold point tropopause (CPT). Panels (c) and (d) show the CHBr₃ vmr (ppt) at these levels. All panels show tropical ($\pm 20°$ latitude) averages over the full simulation period (1993-2012). See Figure 3 for legend. Thick black line denotes multi-model mean.
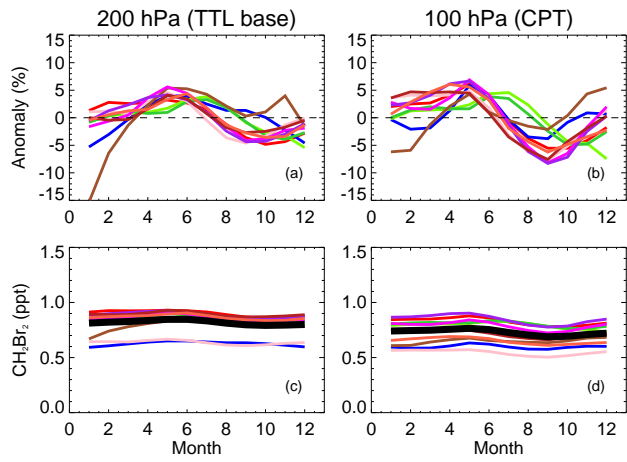
Figure 13. As Figure 12 but for CH$_2$Br$_2$.
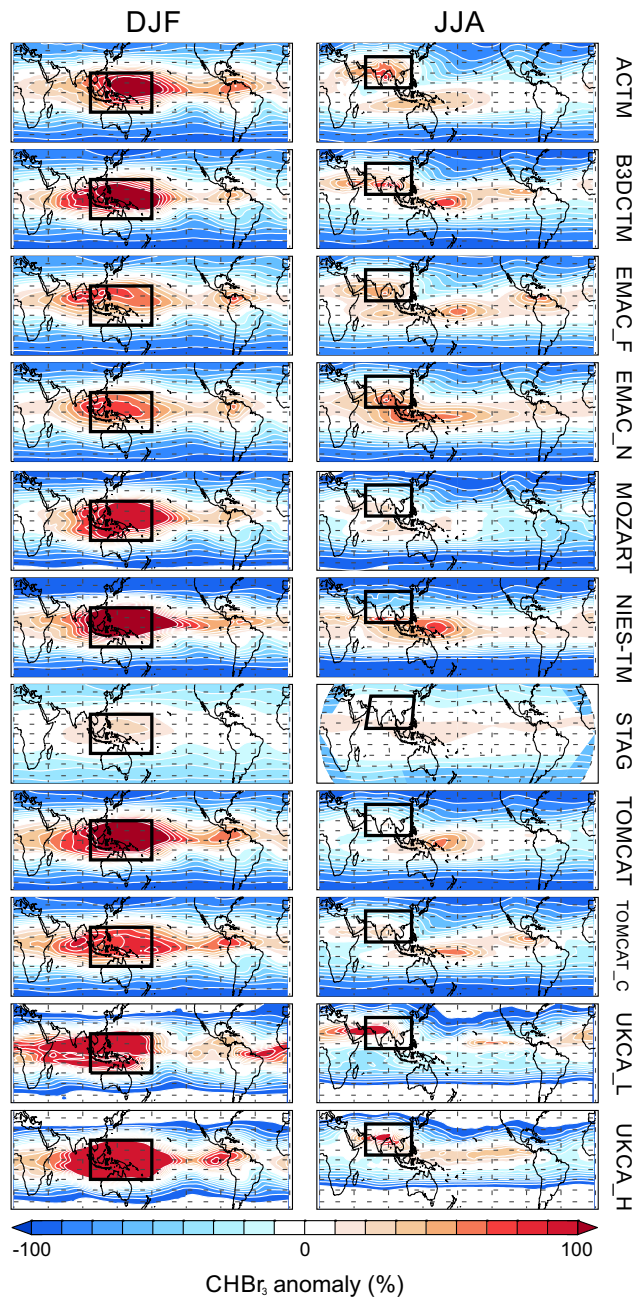
Figure 14. Simulated anomalies of the CHBr$_3$ volume mixing ratio with respect to the tropical ($\pm 30^\circ$ latitude) mean (expressed in %) at 100 hPa for (a) boreal winter (DJF) and (b) boreal summer (JJA). The boxes highlight the tropical West Pacific and location of the Asian Monsoon - regions experiencing strong convection.
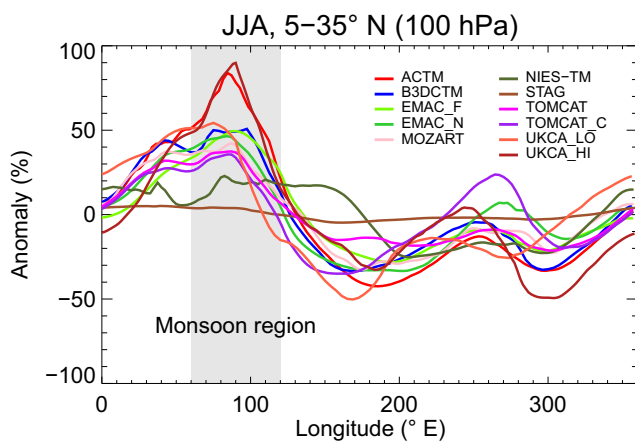
Figure 15. Simulated anomalies of the CHBr$_3$ volume mixing ratio at 100 hPa, as a function of longitude. Expressed as a percentage (%) departure from the mean within the latitude range of the Asian Monsoon (5°N-35°N), during boreal summer (JJA).
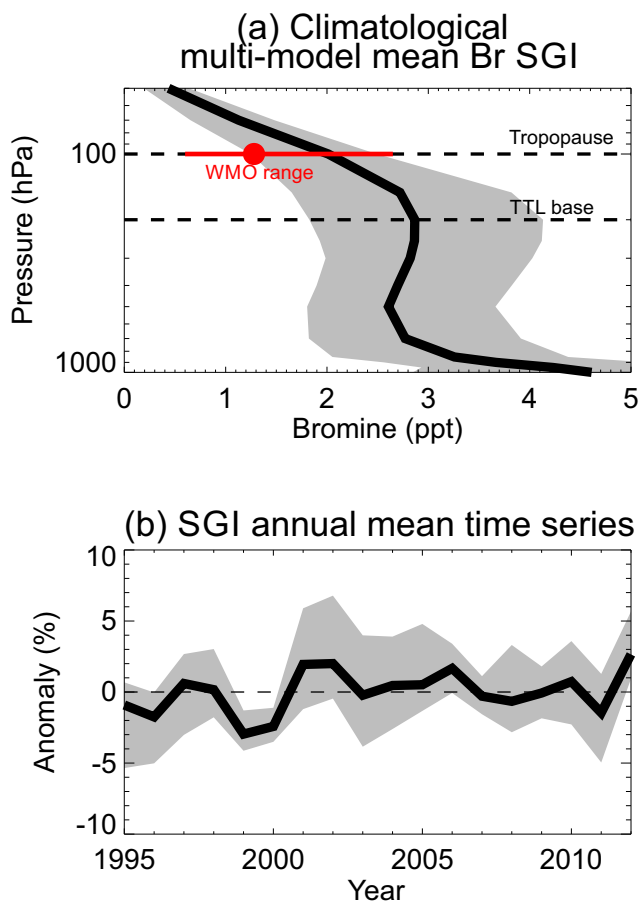
Figure 16. (a) climatological multi-model mean source gas injection of bromine (ppt) from $CHBr_3$ and CH_2Br_2 (i.e. $[3 \times CHBr_3] + [2 \times CH_2Br_2]$ mixing ratio). The shaded region denotes the model spread. Also shown is the best estimate (red circle) and SGI range from these gases (based on observations) reported in the most recent WMO O_3 Assessment Report (Carpenter and Reimann, 2014). (b) time series of multi-model mean stratospheric bromine SGI anomalies. Anomalies are calculated as the departue of the annual mean from the climatological mean (%).
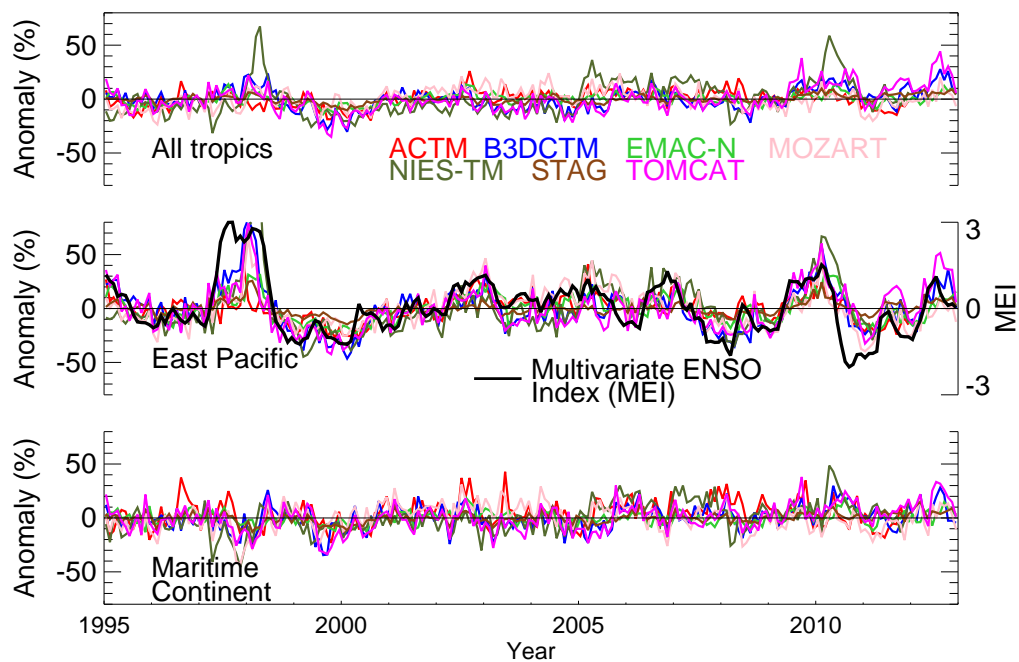
Figure 17. Monthly mean anomalies of CHBr$_3$ volume mixing ratio at 100 hPa, expressed as departures from the climatological monthly mean (%) over (a) tropical latitudes ($\pm 20°$), (b) the tropical East Pacific ($\pm 20°$ latitude, $180°$-$250°$E longitude) and (c) the Maritime Continent ($\pm 20°$ latitude, $100°$-$150°$E longitude). For the East Pacific region, the Multivariate ENSO Index (MEI) is also shown (see text). Note anomalies from free-running models not shown.